ISTITUTO NAZIONALE DI FISICA NUCLEARE

Sezione di Milano

INFN/TC-84/5
13 Marzo 1984

G. Bellomo and L. Serafini: DESIGN OF THE MAGNETIC FIELD FOR THE MILAN SUPERCONDUCTING CYCLOTRON

Servizio Documentazione
dei Laboratori Nazionali di Frascati

Istituto Nazionale di Fisica Nucleare
Sezione di Milano

INFN/TC-84/5
13 Marzo 1984

G. Bellomo and L. Serafini: DESIGN OF THE MAGNETIC FIELD FOR THE MILAN SUPERCONDUCTING CYCLOTRON

INTRODUCTION

The Milan superconducting cyclotron, now under construction at the University of Milan, is a three sectors, three dees machine with an effective $K = 800$ and a $K_{FOC} = 200$. The cyclotron has been designed[1] as a booster for a 15 MV Tandem with ultimate energies between 100 MeV/n for fully stripped light ions down to 20 MeV/n for uranium. Intensities in the range 10^{10}-10^{11} particles/sec are anticipated.

The machine will also be equipped with an internal ion source (of the PIG type) and will have the capability of axial injection from an advanced external ion source (ECR or EBIS).

Status reports on the project, covering all the design aspects of the machine, have been published elsewhere[2].

The machine has a pole radius of 90 cm with a minimum hill gap of 8.6 cm and an average spiral constant of 1/46 rad/cm. Maximum coil excitation is 6.5×10^6 At with operating magnetic fields between 22 and 48 Kgauss. The main machine parameters are listed in Table I.

A vertical cross section of the cyclotron is presented in Fig. 1 while a schematic view of the midplane is shown in Fig. 2. The main components of the machine are indicated together with the beam entry and exit paths.

The operating diagram of the cyclotron in the $(B_o, Z/A)$ plane, i.e. the center field value and the charge to mass ratio of the accelerated ions, is presented in Fig. 3.

TABLE I - Main machine parameters.

Bending limit	K = 800	No. of sectors	3
Focusing limit	K_{FOC} = 200	Av. spiral constant	1/46 rad/cm
Pole radius	90 cm	Min. hill gap	8.6 cm
Yoke inner radius	134 cm	Max. valley gap	91.6 cm
Yoke outer radius	190.3 cm	No. of trim coils	20
Yoke full height	286 cm	No. of dees	3
Total weight	176 tons	RF range	15-48 MHz
Min-Max center field	22-48 Kgauss	Operating harmonics	h = 1, 2, 3, 4
Main coil ampereturns	6.5×10^6 At	Peak dee voltage	100 kV

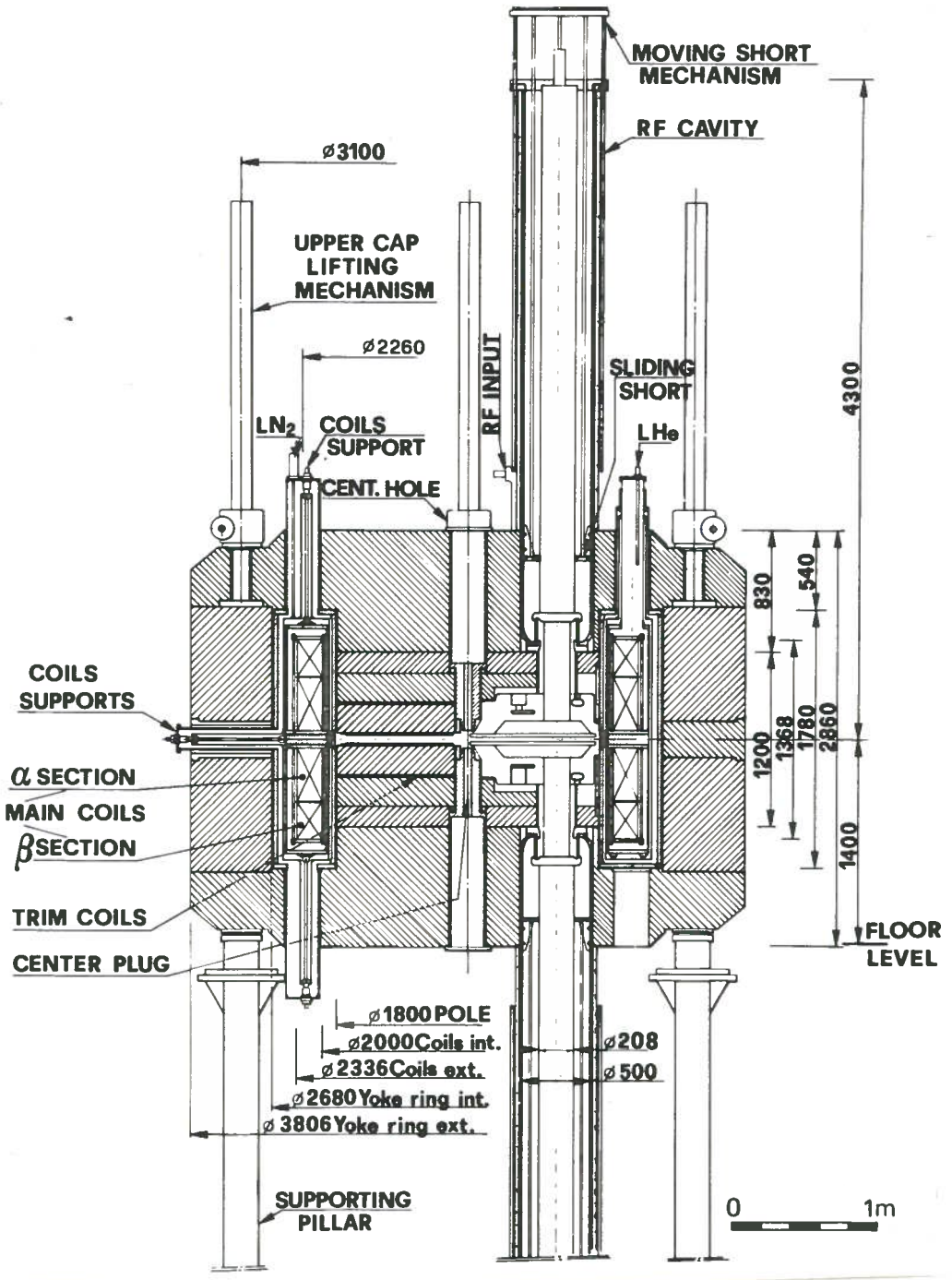

FIG. 1 - Vertical cross section of the cyclotron. All dimensions in mm.

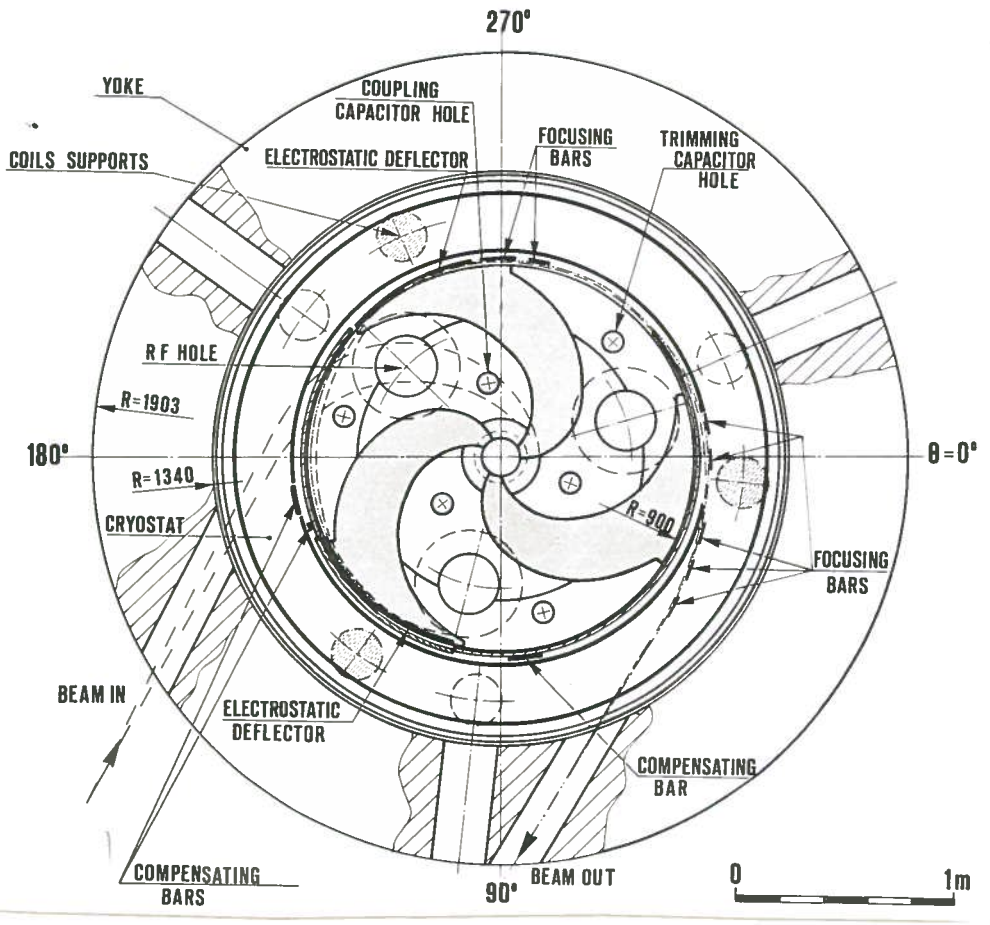

FIG. 2 - Median plane sketch of the cyclotron.

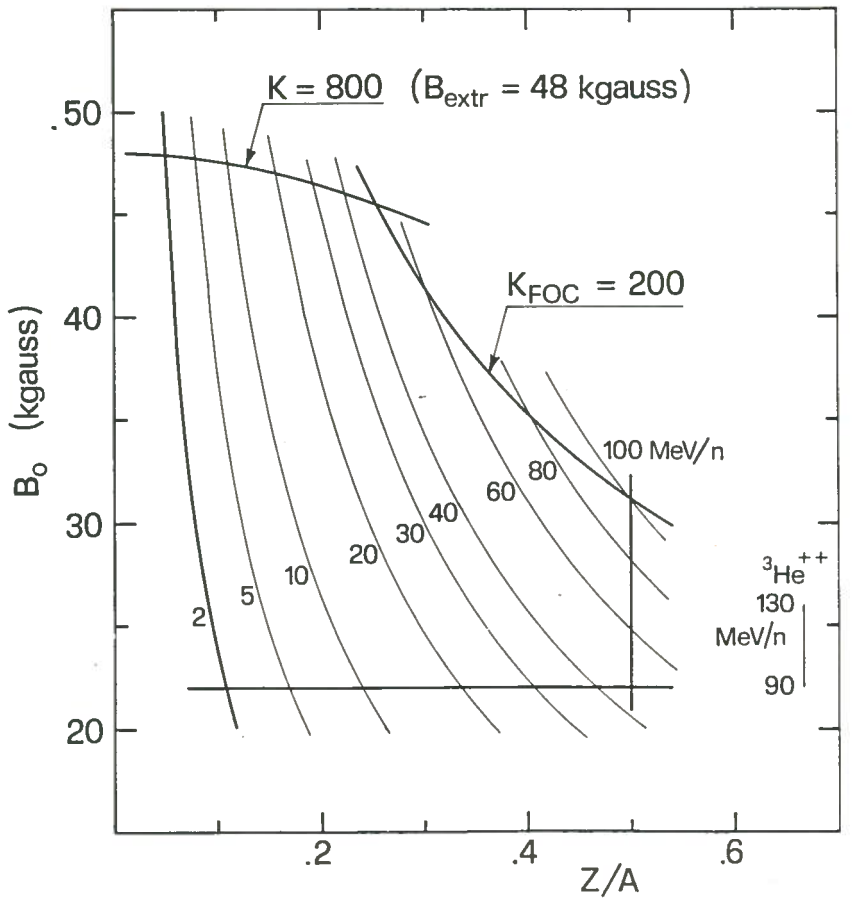

FIG. 3 - Operating diagram of the cyclotron in the (B_o, Z/A) plane.

The bending and focusing limits, together with the constant energy per nucleon lines, are also shown.

The minimum operating field of 22 Kgauss is set by the resonance $\nu_r + 2\nu_z = 3$ while the 2 MeV/n limit represents the minimum energy possible in the h = 4 harmonic mode.

The operating range of the radiofrequency system is 15-48 MHz ; the ions energies are shown in Fig. 4 as a function of the accelerating frequency for the four harmonic modes h = 1, 2, 3, 4 selected.

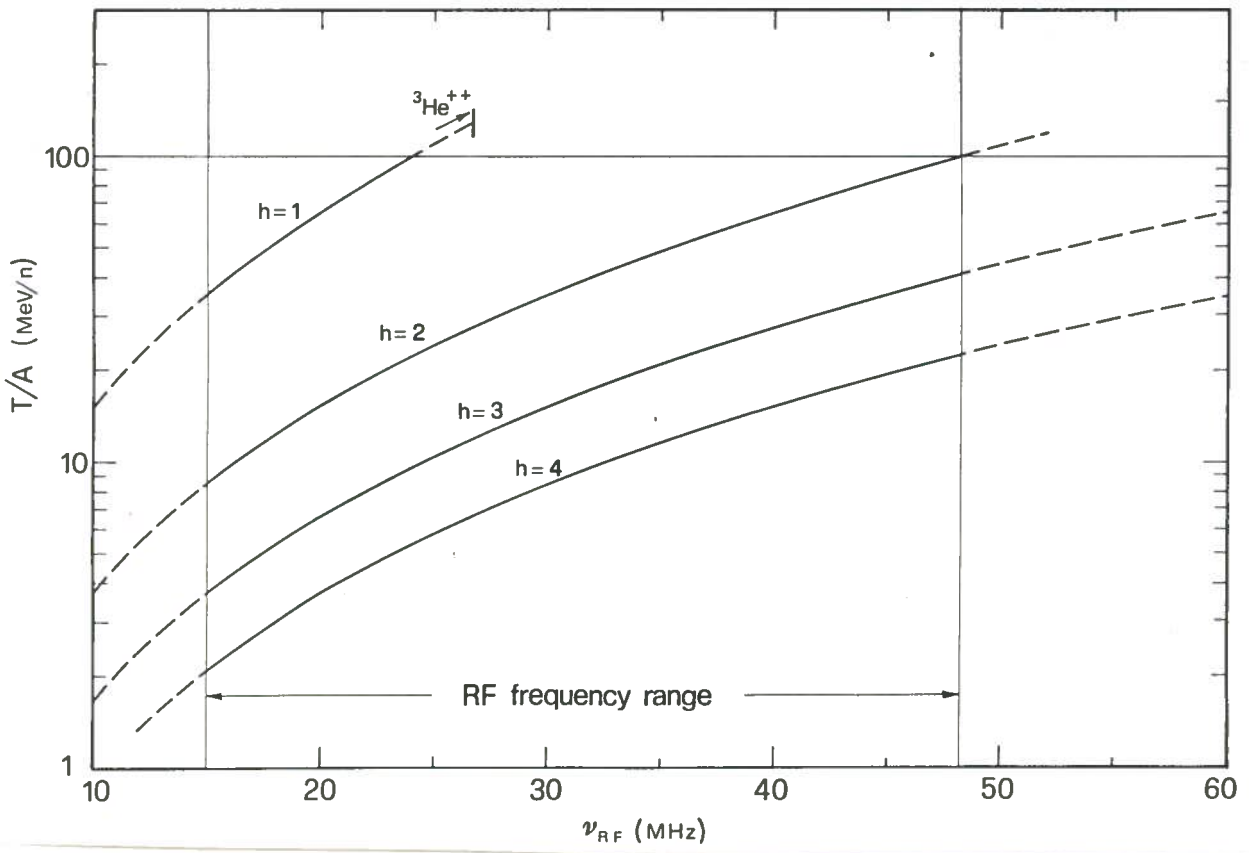

FIG. 4 - Energy vs RF frequency for different harmonic modes.

This paper is intended to give a comprehensive report on the design of the magnetic field and it includes a discussion of the guidelines followed and of the machine performances anticipated on the basis of the calculated field.

The general structure of the machine for all aspects relevant to the magnetic field design, like the iron geometry, the superconducting main coils and the trim coils, is outlined in Section 1.

The design techniques employed are discussed in Section 2 while Section 3 deals with the magnetic field calculations and field characteristics.

The trimming of the field is presented in Section 4 and beam dynamics, as inferred from static equilibrium orbit runs, is discussed in Section 5.

The influence on the beam dynamics produced by the azimuthal field modulation of the trim coils is presented in Section 6 and the control of the first harmonic, necessary for the beam extraction, is treated in Section 7.

1. - GENERAL CHARACTERISTICS OF THE MACHINE

1. 1. - Magnet structure

A vertical cross section of the cyclotron has already been presented in Fig. 1 while a sketch of the magnet top is shown in Fig. 5.

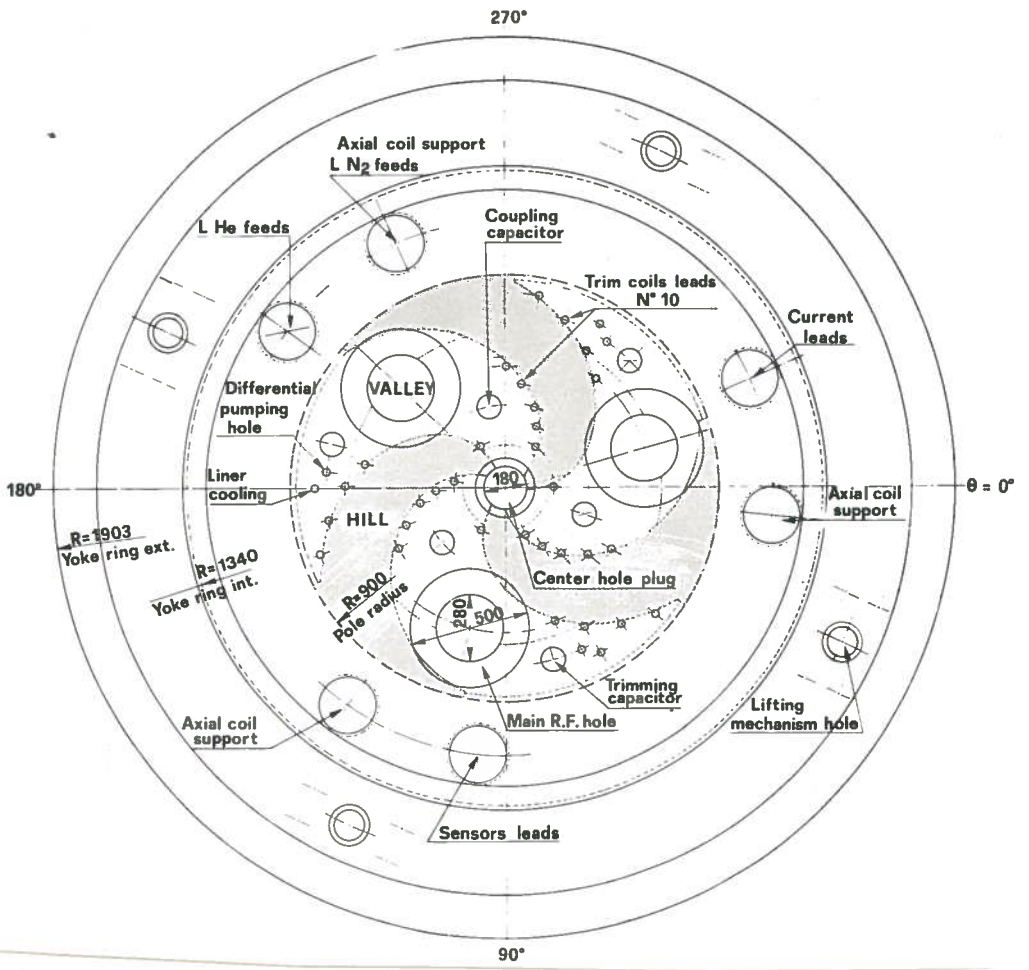

FIG. 5 - Schematic view of the magnet from the top.

The yoke consists of 5 cast steel pieces with a carbon content < 0.01%. The full magnet weight (including sectors) is 176 tons. A detailed description of the magnet structure is given in ref. (3).

The pole forms a single piece with the yoke cap and extends up to 60 cm from the median plane. A 14 cm thick plate, bolted to the pole, supports the sectors and the valley shims whose radial profile is shown in Fig. 6.

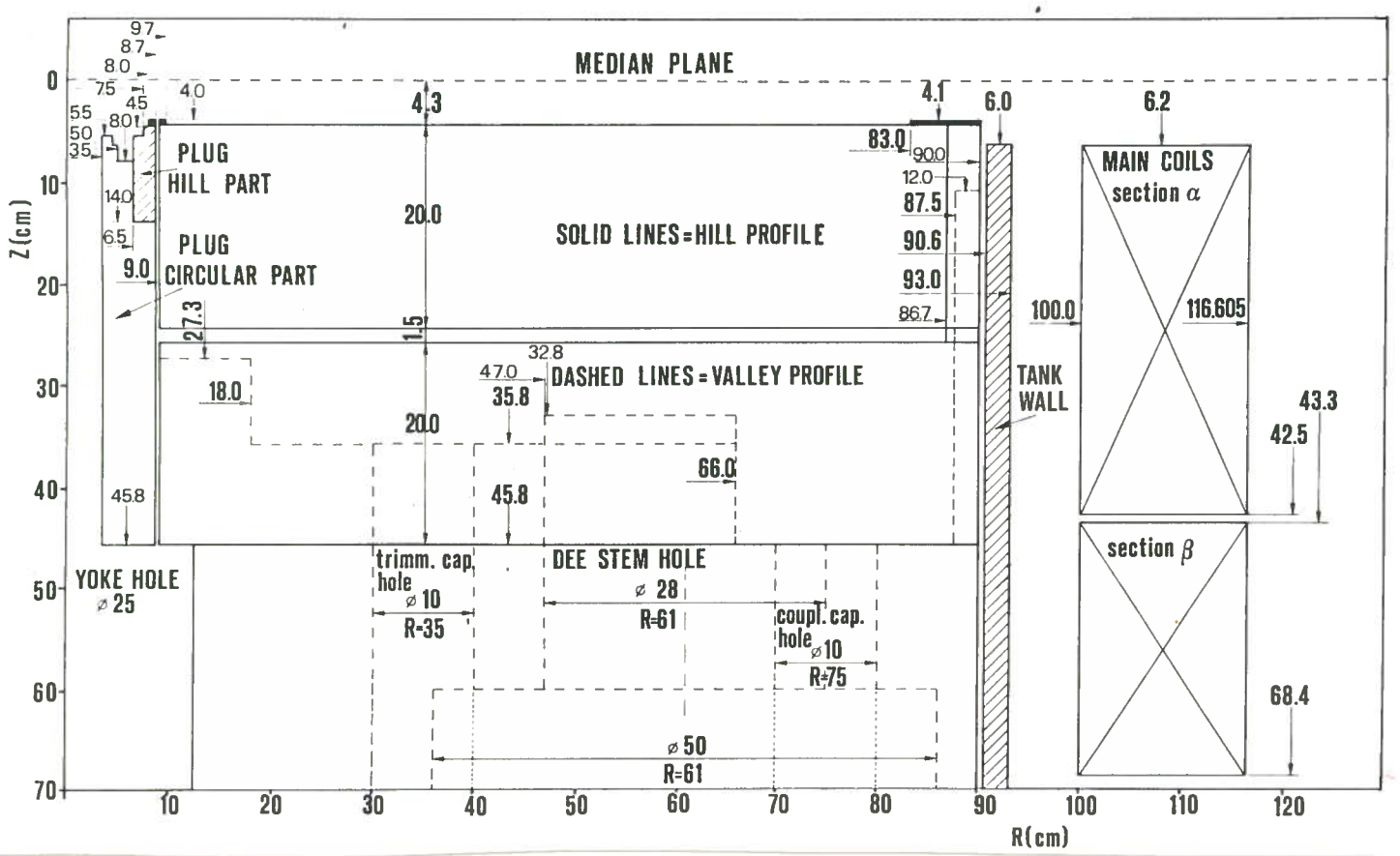

FIG. 6 - Hill and valley radial profiles. All dimensions in cm.

The hill is splitted into two parts, upper and lower, each one 20 cm thick, in order to wind the 20 trim coils around the upper hill (the one closer to the median plane). On the valley floor, at 45.8 cm from the median plane, are placed shims of different height to produce the desired field shape.

A 2.4 cm thick ring, which is the inner wall of the vacuum tank, extends up to 6 cm from the median plane to limit, together with the last shim of the valley (between R = 87.5 and R = 90 cm), the fringing field fall-off.

A center hole of 25 cm diameter is provided in the yoke and in the pole for the insertion of an internal ion source or the axial injection of the beam. The hole diameter is reduced at 7 cm near the median plane by the insertion of a center plug designed to compensate the hole effect on the magnetic field at the midplane.

The plug has an hill part (see Fig. 6) 33^{o} wide which extends the sector up to R = = 6.5 cm. A circular coil of 10 turns, indicated as coil 0, is inserted between R = 5 cm and R = 6.5 cm to control the central cone field (see Section 3).

On each valley, as visible in Fig. 5, three holes are provided for the RF dee stems and the trimming and coupling capacitors. Ten holes are also drilled for the entrance and exit leads of the 20 trim coils since for each group of two trim coils four leads go through the same hole. Two additional holes per valley are used for the pum-

ing in the differential chamber constituted by the RF liner, which will enclose the trim coils, and for the cooling of the liner itself.

The center line of the hill has a spiral constant of 1/45.7 rad/cm between R = = 9 and R = 72 cm and thereafter increases up to 1/31.4 rad/cm at R = 86.7 cm. From R = 86.7 cm to R = 90 cm the hill has no spiral angle in order to better control the onset of the resonance $\nu_r + 2\nu_z = 3$ (see Section 5).

The azimuthal hill width is 33^o at R = 9 cm and reaches 46^o at R = 40 cm being then constant up to R = 72 cm. There the width increases reaching 52^o at R = 86.7 cm and is thereafter constant up to R = 90 cm. The hill is rounded at the edges, from R = = 9 to R = 86.7 cm, with a 20 mm radius of curvature in order to facilitate the winding of the trim coils, which have there a 18 mm radius of curvature.

The upper part of the hill is machined in two pieces. The first one is the spiral sector, i. e. from R = 9 to R = 86.7 cm, the second one is the radial part (R = 86.7 to R = 90 cm).

The valley skirt and the radial part of the lower hill between R = 87.5 and R = 90 cm are machined in a single piece thus forming a solid ring.

Each edge of the spiral sector is defined by three arcs of circle which have, two by two, a common point of tangency. In Table II are listed for each radial zone the center and the radius of curvature of the circles for the two edges (the teta increasing sense is defined as in Fig. 5).

TABLE II - Sectors machining parameters.

R (cm)	Edge 1 r_c (cm)	Edge 1 ϑ_c (deg)	Edge 1 ϱ (cm)	Edge 2 r_c (cm)	Edge 2 ϑ_c (deg)	Edge 2 ϱ (cm)
9-40	29.000	- 4.245	31.313	28.787	47.902	28.201
40-72	37.466	-37.041	51.759	37.466	8.959	51.759
72-86.7	36.850	-40.666	54.189	38.878	-30.018	77.264

R Radial position on the edge respect to the center of the machine.
r_c, ϑ_c Polar coordinates of the arc center respect to the center of the machine.
ϱ Radius of curvature of the arc of circle.

The azimuthal position of the hill edges and the hill width are given, as a function of radius, in Table III.

TABLE III - Hill profiles.

R (cm)	ϑ_1 (deg)	ϑ_2 (deg)	$\Delta\vartheta$ (deg)
9.0	92.19	125.19	33.00
10.0	89.66	124.54	34.88
12.0	85.39	123.06	37.67
14.0	81.77	121.40	39.63
16.0	78.54	119.62	41.07
18.0	75.58	117.75	42.17
20.0	72.78	115.81	43.03
22.0	70.09	113.81	43.72
24.0	67.48	111.75	44.27
26.0	64.92	109.63	44.72
28.0	62.37	107.45	45.08
30.0	59.84	105.21	45.37
32.0	57.29	102.89	45.60
34.0	54.73	100.50	45.77
36.0	52.12	98.02	45.90
38.0	49.47	95.44	45.97
40.0	46.74	92.74	46.00
42.0	44.03	90.03	46.00
44.0	41.40	87.40	46.00
46.0	38.84	84.84	46.00
48.0	36.34	82.34	46.00
50.0	33.88	79.88	46.00
52.0	31.45	77.45	46.00
54.0	29.04	75.04	46.00
56.0	26.64	72.64	46.00
58.0	24.24	70.24	46.00
60.0	21.82	67.82	46.00
62.0	19.39	65.39	46.00
64.0	16.93	62.93	46.00
66.0	14.43	60.43	46.00
68.0	11.87	57.87	46.00
70.0	9.25	55.25	46.00
72.0	6.53	52.53	46.00
74.0	3.72	49.79	46.07
76.0	0.80	47.10	46.30
78.0	- 2.27	44.43	46.70
80.0	- 5.53	41.79	47.32
82.0	- 9.03	39.17	48.20
84.0	-12.89	36.55	49.44
86.0	-17.28	33.92	51.20
86.7	-19.00	33.00	52.00
88.0	-19.00	33.00	52.00
90.0	-19.00	33.00	52.00

1. 2. - The superconducting coils

A cross section of the main coils is shown in Fig. 7 and their main characteristics are listed in Table IV.

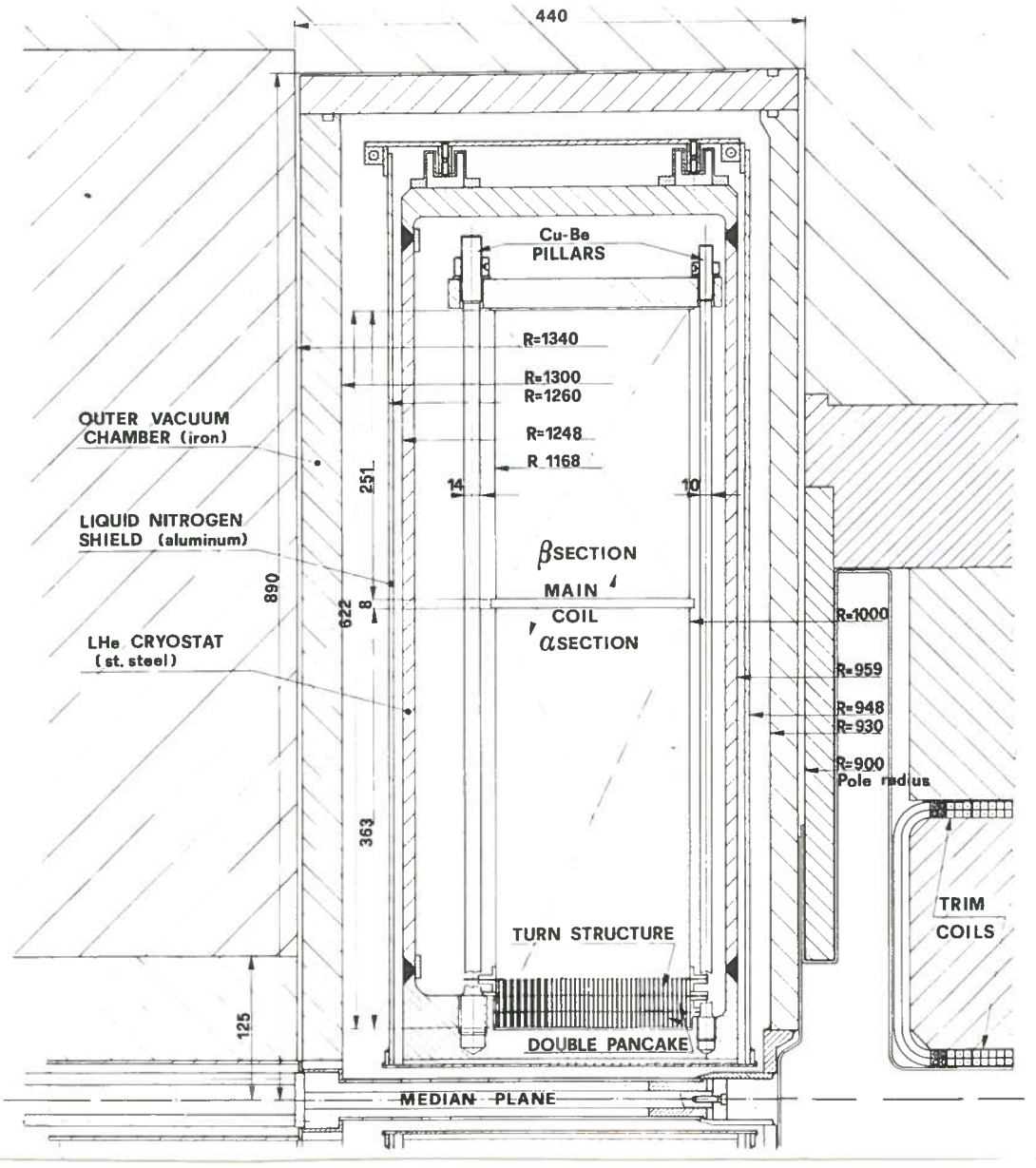

FIG. 7 - Main coils cross section. All dimensions in mm.

TABLE IV - Main coils parameters.

Max Ampereturn	6.5×10^6	Cable dimensions	13×3.5 mm^2
Max overall density	3500 A/cm^2	Overall Cu/Sc ratio	20 : 1
Internal radius	100 cm	Superc. insert	monolithic NbTi
External radius	116. 8 cm	Insert dimensions	1.8×3.6 mm^2
Min. dist. from midplane	6. 2 cm	Insert Cu/Sc ratio	2 : 1
Height of section α	36. 4 cm	Number of filaments	540
Height of section β	25. 2 cm	Filaments diameter	70 μm
Number of turns	38	Twisting pitch	25 mm
Layers in α section	2 x 13	Nominal current	2000 A
Layers in β section	2 x 9	Crit. current (B = 5 T, T = 4.2°K)	2700 A

The main coils are splitted in two sections, labelled as α and β, the α section being the one closer to the median plane. The two sections are independently excited for the trimming of the magnetic field up to a maximum overall density of 3500 A/cm^2, corresponding to 6.5×10^6 At. The fields produced by the two coil sections at the maximum excitation are presented in Fig. 8 where the coil dimensions are also indicated.

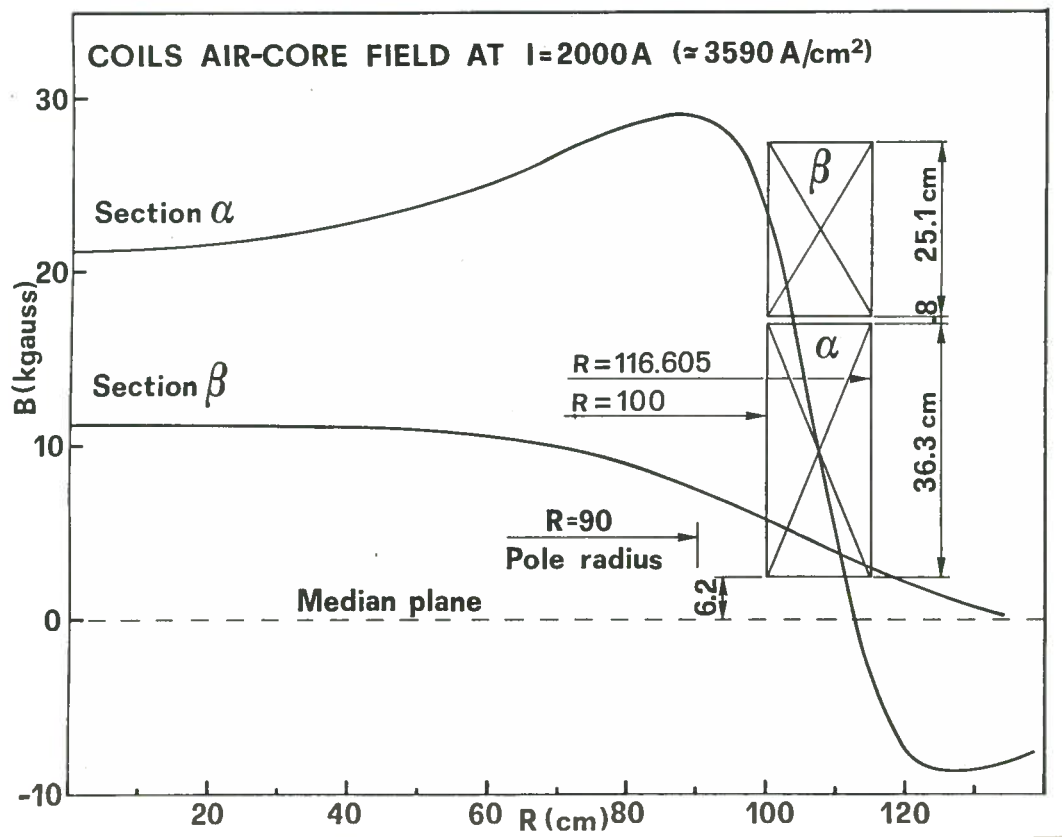

FIG. 8 - Air-core fields of the two main coils sections at the indicated current density.

The coils are in a liquid helium bath at atmospheric pressure ($T = 4.2^oK$): a consumption of 15 l/h of LHe and 15 W is anticipated. The main features of the cryostat, liquid nitrogen shield and vacuum chamber are shown in Fig. 7.

The coils are wound with the double pancake technique and consist of 38 turns of 26 layers in the α section and 18 layers in the β section. The cable has dimensions of 13×3.5 mm^2 with a superconducting NbTi insert of 1.8×3.6 mm^2. The copper to superconductor ratio is 2:1 in the insert and 20:1 overall. The nominal current, corresponding to the average density of 3500 A/cm^2, is 1944 A. The cable critical current at B = 5 T is in excess of 2700 A.

The maximum current density is 3500 A/cm^2 for both sections: the β section has to be excited in opposition to the α section up to -1500 A/cm^2 for the acceleration of fully stripped ions (see Section 2). In order to prevent the axial lifting of the β section the pancakes are compressed to approximately 700 tons by copper berillium tie

rods as indicated in Fig. 7. More details on the coils and cryostat design can be found on ref. (4).

1. 3. - The trim coils

The twenty trim coils are wound on the upper part of the hill and are packed in five groups, of 4 coils each, separated by radial spacers which also support the hill as indicated in Fig. 9.

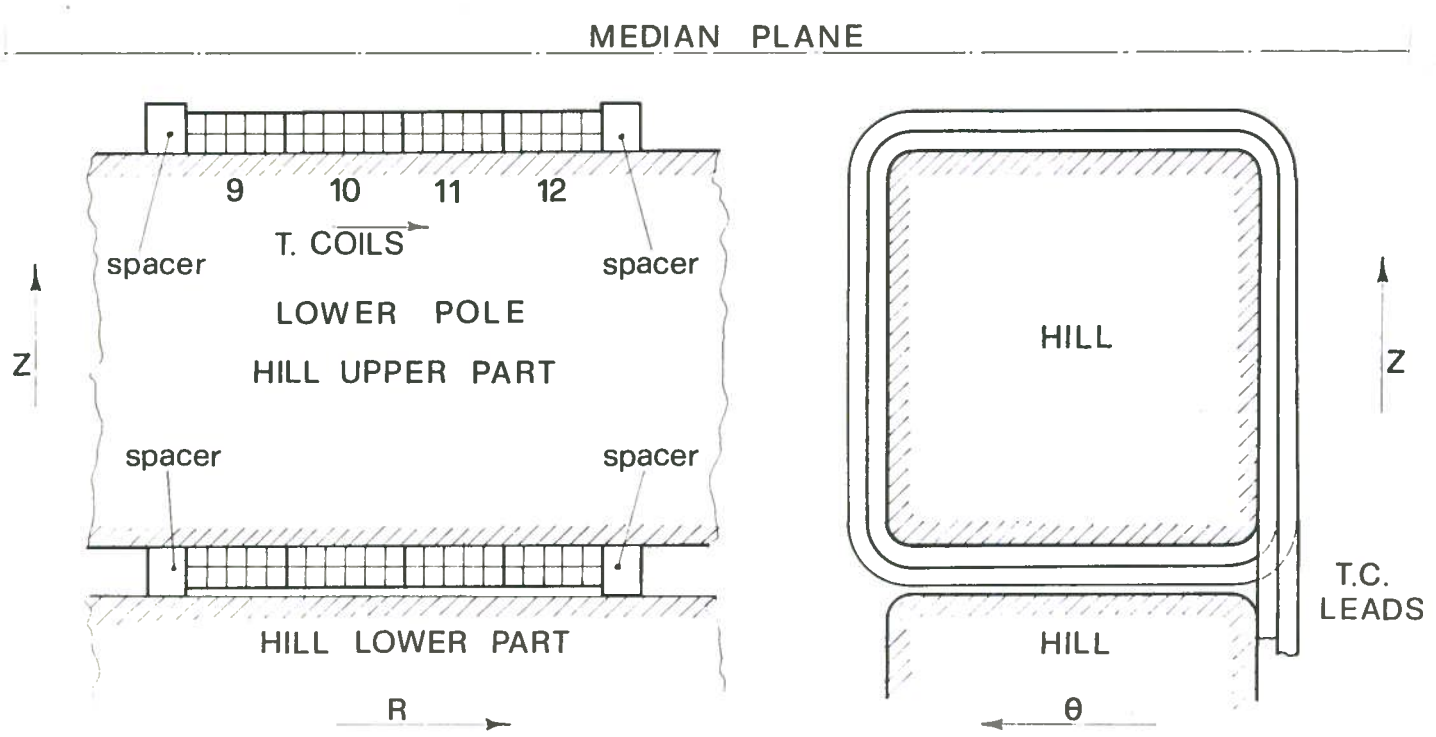

FIG. 9 - Schematic view of a group of four trim coils.

Each trim coil consists of two layers with a variable number of turns to fill up completely the region between the spacers. The last T. C. has only one layer to allow the inward movement of the electrostatic deflector (see Section 5).

The entrance and exit leads lay on the same side of the hill, so that for each group of two trim coils four leads go through the same hole in the valley floor (see Fig. 5).

The trim coils are wound with 1/4" square hollow (hole diameter = 3/16") copper conductor which, when water cooled, can carry up to 500 A. The group of 4 coils closest to the center has however a 3/16" square hollow (hole diameter = 1/8") conductor in order to limit the azimuthal extent of the trim coils on the hill side. This will allow a gap to gap azimuthal width between the dees as close as possible to the design value of 60 degrees.

Trim coils number (1, 2) or (3, 4) and (19, 20) will be used also as harmonic coils to control the first harmonic in the injection and the extraction regions. The

maximum excitation needed for the trimming of the field has been calculated in 4000 At per winding and about 1600 At are required for them to operate as harmonic coils. The magnetic forces acting on the trim coils have been evaluated in order to design a proper mechanical structure (see ref. (5)).

The main characteristics of the trim coils are listed in Table V. The form factors of a few trim coils in the trimming mode operation at 3000 At of excitation (T. C.

TABLE V - Trim coils geometry.

T. C.	Rav (cm)	R_i (cm)	R_F (cm)	$\Delta\vartheta$ (deg)	Nt	I (A)	Notes
		9.00	9.80				Spacer 0
1	11.59	9.80	13.38	42.1	14	400	
2	15.17	13.38	16.95	44.3	14	400	Harmonic coils
3	18.74	16.95	20.53	45.6	14	400	Conductor 3/16"
4	22.32	20.53	24.11	46.5	14	400	
		24.11	25.41				Spacer 1
5	27.08	25.41	28.76	48.0	10	400	
6	30.77	28.76	32.77	48.3	12	330	
7	34.45	32.77	36.12	48.5	10	400	
8	37.80	36.12	39.47	48.5	10	400	
		39.47	40.77				Spacer 2
9	42.46	40.77	44.14	48.4	10	400	
10	46.16	44.14	48.19	48.2	12	330	
11	49.87	48.19	51.56	48.1	10	400	
12	53.24	51.56	54.93	48.1	10	400	
		54.93	56.23				Spacer 3
13	57.92	56.23	59.60	48.0	10	400	
14	61.62	59.60	63.65	47.9	12	330	
15	65.33	63.65	67.02	47.9	10	400	
16	68.70	67.02	70.39	48.0	10	400	
		70.39	71.69				Spacer 4
17	73.38	71.69	75.08	48.1	10	400	
18	76.77	75.08	78.47	48.5	10	400	
19	80.50	78.47	82.53	49.7	12	460	Harmonic coil
20	84.57	82.53	86.60	51.1	6	500	Harmonic coil, one layer
		86.60	87.90				Spacer 5

Rav — Average radius of the trim coil.
R_i, R_F — Initial and final trim coil radii.
$\Delta\vartheta$ — Average azimuthal width of the trim coil.
Nt — Number of turns of the trim coil.
I — Maximum excitation current (trimming and harmonic operation mode).

20 at 1500 At) are presented in Fig. 10.

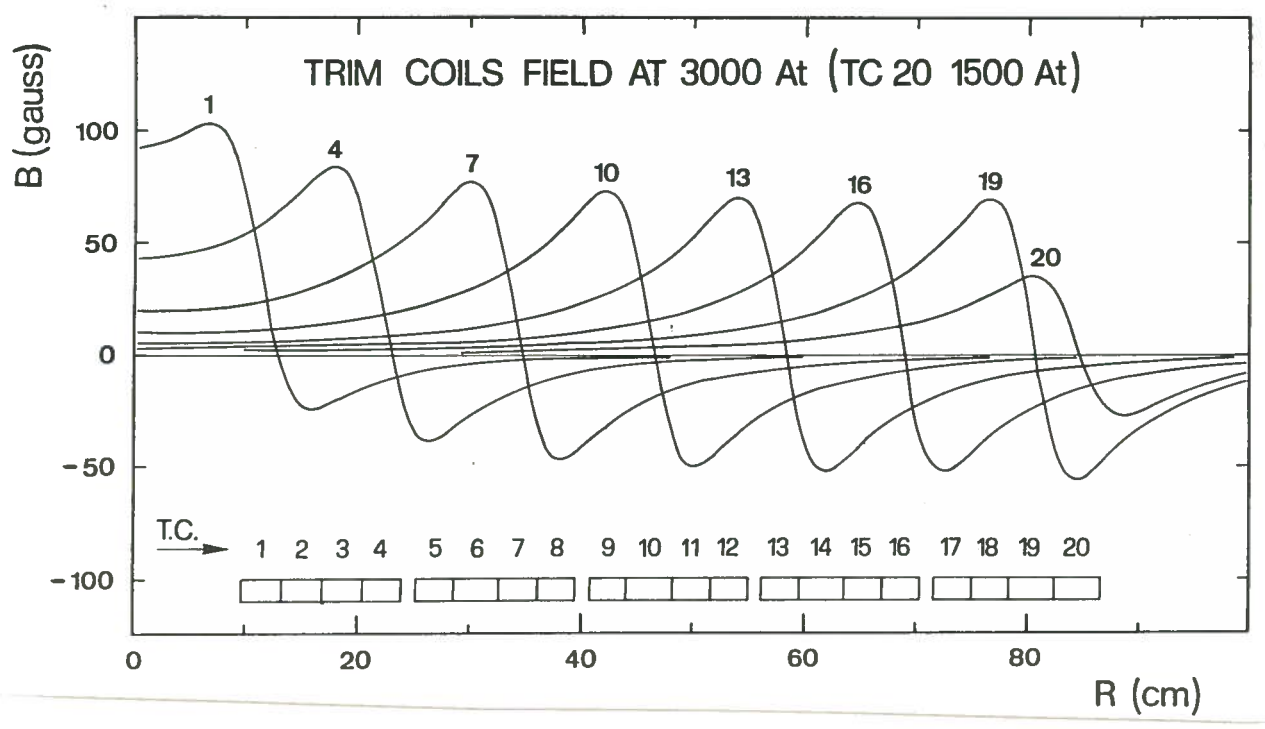

FIG. 10 - Air-core average fields for few selected trim coils. The geometry of the trim coils is schematically indicated at the bottom.

2. - DESIGN CONSIDERATIONS

2. 1. - Historical notes on the project

The design study for the superconducting cyclotron started in 1975, the machine being intended as a booster for a 16 MV Tandem. The study was completed at the beginning of 1976 and a proposal was submitted to the National Institute for Nuclear Physics (INFN) for a $K = 500$, $K_{FOC} = 120$ machine. A detailed description of that project is given in ref. (1).

In 1977, pending the approval and funding of the project, a program was set up for the construction of a 1 : 6 superconducting model magnet and a 1 : 1 RF cavity model.

This program was terminated in 1978 with the successful operation of the models whose result have been extensively reported[6].

Lack of funding prevented the continuation of the project until the end of 1980 when the construction of the machine was approved and funded.

In 1980, close to the start up of the project, a complete review of the design was undertaken. The rationale for a new design was the certainty to improve the machine performances. This goal was justified by the experience aquired, in the superconducting and cryogenic technology with the model program as well in the magnetic field and

RF design. Such an improvement in performances was to be obtained at essentially the same capital cost of the machine.

Consequently the following constraints, mutuated from the original proposal, were kept:

- Pole radius R = 90 cm.
- Maximum main coils excitation 6.5×10^6 At.
- Coupling with the Tandem with a 4 : 1 energy variation.

The first two constraints actually limit the size of the magnet and of the superconducting coils i. e. two of the major cost items.

The main changes in the design and the way to obtain them are summarized below:

- An increase of the bending limit to K = 800 obtained by placing the coils closer to the midplane and to the pole. The maximum operating field was therefore increased from 41 to 48 Kgauss.
- An increase of the focusing limit to $K_{FOC} = 200$ obtained with a spiral constant of 1/46 rad/cm vs the original value of 1/59 rad/cm.
- A cylindrical yoke structure, as opposed to an open three-fold structure in order to decrease both the stray fields and the magnet weight.
- A change of the RF frequency and corresponding harmonic modes i. e. 15-48 MHz, h = 1, 2, 3, 4 vs the 21-63 MHz, h = 3, 9 previously envisaged.
- Coupling to the Tandem using a higher stripper ratio Zs/Zi from an average of 3-3.5 to 3.5-4 (Zi, Zs charge state of the ion before and after the stripping into the cyclotron).

The guidelines followed in the design of the main coils and of the sectors will be presented in the next paragraph. The injection of the beam into the cyclotron and its coupling to the Tandem will be described in a forthcoming paper[7].

2. 2. - Design guidelines

The performances of a superconducting cyclotron depend both on the main coils and on the iron geometry since the coils provide up to 2/3 of the total magnetic field. The two aspects are covered separately and their interdipendence will be pointed out.

For the NbTi superconducting cable it is customary to assume as optimal a maximum magnetic field of 5 Tesla with a corresponding critical current density, in the superconductor, of $\sim 10^5$ A/cm^2. The cryostabilization of the cable, i. e. the insertion of the superconductor into a copper matrix, limits the average current density to $\simeq 5000$ A/cm^2. Safety margin on the critical current and the filling factor of the coils

set the maximum overall current density at 3500 A/cm^2.

Note that the 5 T max field on the coils corresponds approximately to the max field level on the midplane and therefore the bending limit of the machine is determined by this field value and by the extraction radius.

To reach the 5 T field level and the proper radial field shape the coils must be placed as close as possible to the midplane and to the pole. The inner radius of the coils and the minimum distance from the midplane were set respectively to R = 100 cm and z = 6.2 cm, as allowed by the design of the cryostat and by the radial penetrations needed for the extraction elements.

The inner wall of the vacuum chamber is made out of iron so that the "magnetic" pole radius is 93 cm as opposed to the geometric value of 90 cm. This feature provides a 7% increase in the bending limit and helps in bringing the coils radially closer to the "magnetic" pole.

The bending limit of the machine was eventually set at K = 800 corresponding to a max field B = 4.8 T and to an extraction radius of approximately 85 cm. We recall that the bending limit of the cyclotron is defined by the relation

$$T/A \leqslant K(Z/A)^2$$

between the final energy and the charge to mass ratio of the accelerated ions with

$$K = \frac{e^2 B^2 R^2}{2m_o}$$

where B is the max magnetic field at the extraction radius R and m_o is the atomic mass unit ($m_o c^2$ = 931.5 MeV).

The coils should also provide a rather sharp fringing field fall-off to facilitate the beam extraction. This requirement again calls for coils placed as close as possible to the pole and to the midplane and for a high aspect ratio H/W (height/width) of the coils cross-section. The selected values, compatible with all the constraints of the coil construction, are H = 60 cm and W = 16 cm.

Furthermore the coils have to be splitted in two sections, independently excited, to provide the field isochronization. The trim coils, being wound on the hills, have a low efficiency and give a field contribution limited to a few hundred gauss.

The coils splitting has therefore the aim of minimizing the trim coils power, while providing the required field level and isochronous shape, together with an acceptable fringing field.

The same requirements with respect to the T. C. power and fringing field must be met by the iron generated field whose radial behaviour is mainly dependent on the

sectors shape. Specifically the iron field, in conjunction with the coils splitting, should also minimize the T. C. power needed for field isochronization.

The primary goal of the sector design is however to assure an adequate axial focusing for the accelerated beam. We recall that the focusing limit of a superconducting cyclotron is to a first approximation described by:

$$T/A \leq K_{FOC}(Z/A)$$

with

$$K_{FOC} = \frac{eRc}{2}\sqrt{C^2(1+2\,tg^2\gamma)}$$

where R is the extraction radius, C is the main harmonic of the azimuthal modulation and $tg\,\gamma$ is the spiral focusing term.

The harmonic C is determined by the hill and valley gap and is of the order of 7-8 Kgauss for reasonable gap values. The focusing limit is therefore mainly dependent on the spiral term and increases almost linearly with the spiral constant.

A limit is set however by the reduced spiral efficiency since in reality the magnetic focusing term $tg\,\gamma$ does not increase as the geometric one for high values of the spiral constant (see Section 3).

The beam extraction process sets a further limit to the maximum achievable energies. Since extraction is accomplished with electrostatic deflectors the upper limit for the electric field defines a relation similar to the focusing one namely

$$T/A \leq K_{extr}(Z/A)$$

where K_{extr} depends on the details of the extraction i. e. number and length of the deflectors, maximum electric field considered, behaviour of the fringing field, etc.

For the Milan machine the beam extraction[8] is obtained with two electrostatic deflectors positioned in two consecutive hills followed by a set of passive magnetic channels. With the present magnetic field configuration and extraction scheme the extraction limit can be set at $K_{extr} = 200$, a value which matches the focusing limit $K_{FOC} = 200$.

Margin has however been provided on the focusing limit since the minimum axial focusing frequency is in excess of $\nu_z = 0.15$ vs the customary accepted value of $\nu_z = 1$.

The high value of the flutter and of the spiral term, in conjuction with the sharp fringing field fall-off, pushes the axial focusing frequency near extraction to values over $\nu_z = 1$ and resonance lines are therefore approached or crossed. For a three sectors machine the intrinsic resonance $\nu_r + 2\nu_z = 3$ is particularly dangerous since it

causes an axial beam loss. Reduction of the vertical focusing in the extraction region has been obtained by imposing a radial shape to the sectors between R = 86.70 cm and R = 90 cm.

This is a compromise between the requirement of high spiral focusing in the region around R = 81 cm (where the axial focusing reaches the minimum values) and low spiral focusing in the extraction region i. e. R = 85 cm.

At the low field levels however, due to the increase of the flutter, the resonance cannot be avoided and therefore a minimum operating field level exists at B_o = 22 Kgauss. At this field level the extraction must take place at rather inner radii in order to avoid the resonance (see Section 5).

2. 2. - Trim coils power minimization

Isochronization of the magnetic field, as previously mentioned, must be obtained with the independent excitation of two coils sections since the trim coils field correction capability is limited to a few hundred gauss.

Twenty trim coils are wound around the upper part of the hill (see Section 1). This number is a compromise between the efficiency, related to the residual r. m. s. field error, and the cost and the design complexity of a large number of trim coils.

The optimal splitting of the coils, with the corresponding optimal iron field, must minimize the trim coils power throughout the operating range of the machine. A low T. C. power implies small residual field errors and consequently negligible oscillations in the phase curve and in the focusing frequencies for the accelerated ions.

A procedure to compute the optimal coils splitting and the corresponding iron field shape, is described in detail in ref. (9). An improved version, which can take into account the variation of the iron field with the main coils excitation, has been implemented.

Essentially the procedure allows to minimize, for a given set of trim coils and for a selected coils splitting, the T. C. power and the r. m. s. field error for the two most difficult ions to isochronize. The latter are generally the most energetic ion at the lowest field ($Z/A = 0.5$, B_o = 22 Kgauss for the Milan machine) and the least energetic ion at the highest field ($Z/A = 0.05$, B_o = 48 Kgauss).

The minimization implies a particular radial behaviour of the iron produced field, which is named B_{best}. Its level and radial slope can be chosen as parameters to match the actual iron field as close as possible. The trim coils will operate symmetrically in the field isochronization of the two selected ions providing equal and opposite field contributions. The trim coils power requirement will be lower for all

the other ions of the operating diagram of the machine for a well behaved dependence of the iron field as a function of the main coils currents. In particular there is a zero power line crossing the operating diagram (see ref. (9) and Section 5). The coils splitting is defined with the fraction parameter $F = h\alpha/(h\alpha + h\beta)$ where $h\alpha$, $h\beta$ are the height of the two sections (the α section being closer to the midplane).

The conclusions drawn in ref. (9) concerning the coils splitting, derived in the design of the MSU K800 cyclotron, have been confirmed also for the Milan machine. Specifically the T. C. power decreases with increasing values of the fraction F; this power decrease requires however to run the upper coil (β section) at progressively lower currents and ultimately to a reverse sign with respect to the α section. In this case the β section is radially compressed and pushed away from the median plane and therefore a special design of the coil structure is required to prevent the axial lifting and the buckling of the β section.

A reasonable compromise between a low T. C. power and the max negative current in the β coil which can be tolerated is reached for a partition fraction of the order of $F = 0.6$, value which has been selected for the Milan machine.

The corresponding optimal iron field B_{best} has been calculated and the sector geometry designed in order to meet this field as close as possible. The final result of such an iterative process is presented in Fig. 11 where, for the indicated main coils excitation, the B_{best} field and the actual iron field are compared. As visible from the figure the agreement is remarkable, i. e. ± 10 gauss at all radii.

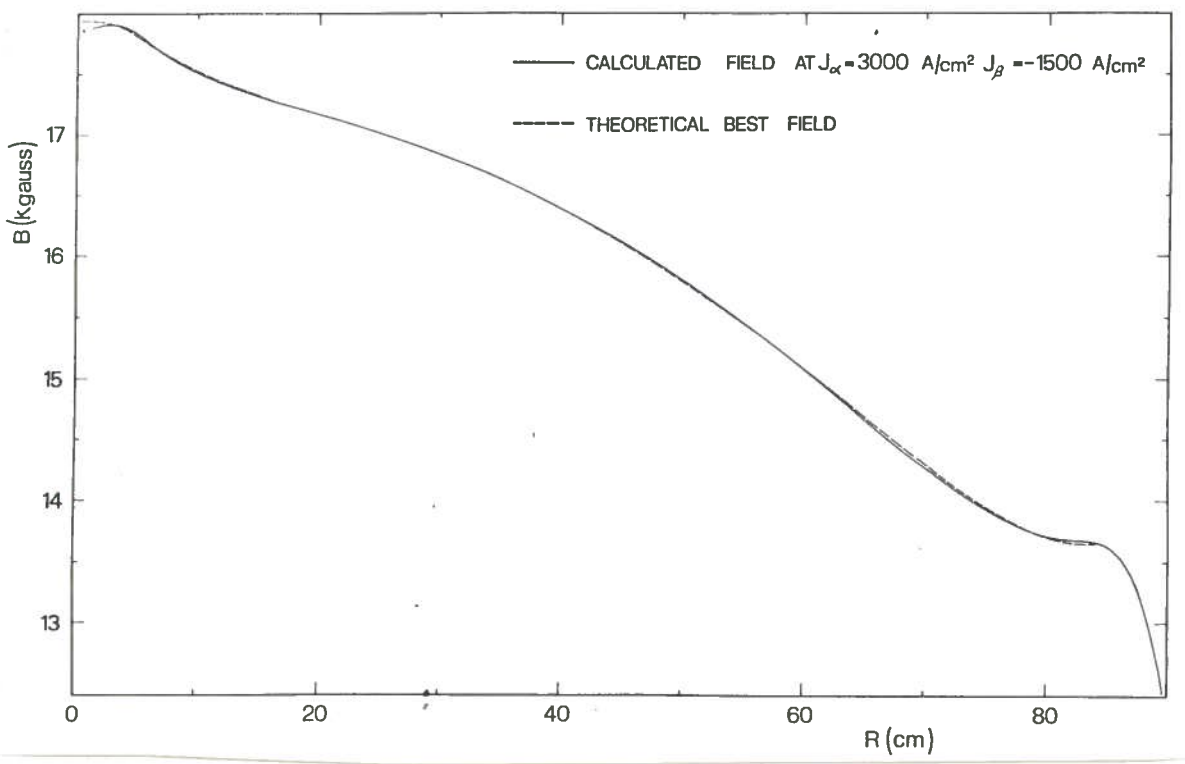

FIG. 11 - Average field produced by the iron compared with the theoretical best field.

A value of 3.5 Kgauss has been selected for the B_{best} field slope, here defined as $B_{best}(r=20) - B_{best}(R=80)$, to limit the maximum current density in the coil sections to $J = 3500\ A/cm^2$. Increase or reduction of the iron field slope causes infact, for the field isochronization of any given ion, a correspondent increase of reduction of the α section current and viceversa for the β section current. Proper choice of the iron field slope can therefore be used to obtain the same maximum current density in the two sections for the given operating range of the machine.

The sector shape which produces the B_{best} field was obtained in three successive steps:

- Shimming of the valley floor between R = 9 and R = 66 cm in order to obtain the required iron field slope.
- Increase of the hill width up to $\Delta\vartheta = 52^o$ at R = 87 cm, starting from $\Delta\vartheta = 46^o$ at R = 72 cm, to match the B_{best} flat shape near extraction. A shim of 2 mm thickness is also placed on the hill top between R = 83 cm and R = 90 cm.
- Small additional shimming of the valley to match the B_{best} shape in the midregion of the machine (R < 70 cm).

The operating diagram of the machine in the (I_α, I_β) plane is presented in Fig. 12. Bending and focusing limits, together with the lines of constant center field B_o and charge to mass ratio Z/A, are shown. The maximum current density of 3500 A/cm^2 is reached for each section along the bending limit. Negative excitation of the β section at 1000 A/cm^2 is necessary for the acceleration of the fully stripped ions and approximately 2000 A/cm^2 is required for the He beams. Trim coils power requirements are described in Section 4 where typical trim coils field contributions and currents setting are presented.

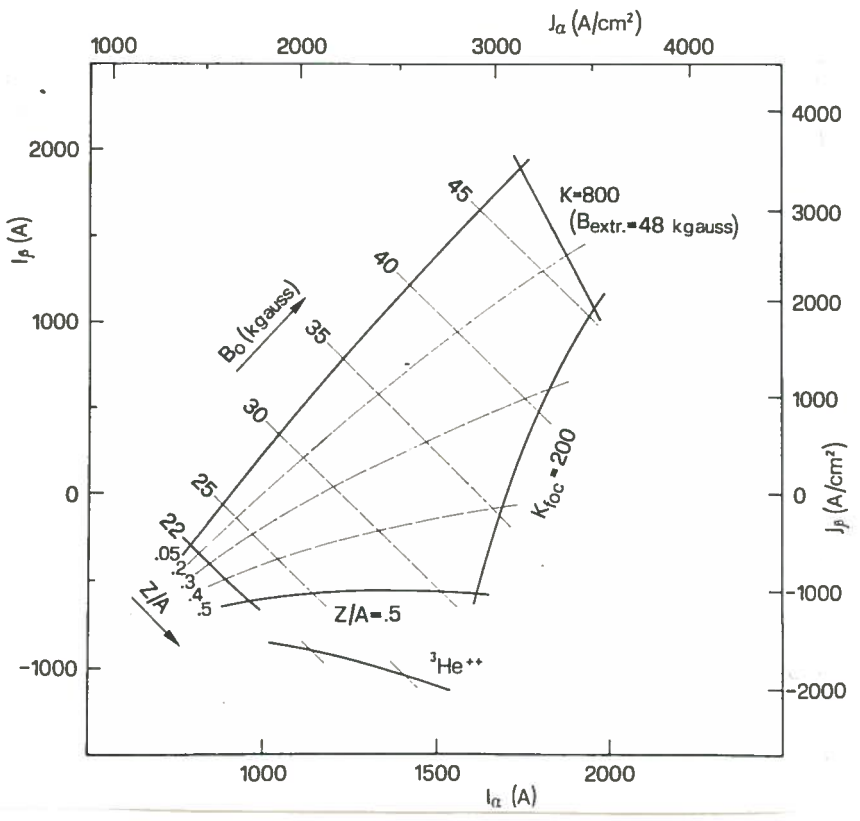

FIG. 12 - Operating diagram of the cyclotron in the (I_α, I_β) plane.

3. - MAGNETIC FIELD CHARACTERISTICS

3. 1. - Field calculation

The total magnetic field on the median plane of a cyclotron is considered as the sum of the following three terms:

$$B(r,\vartheta) = B_G(r) + B_S(r,\vartheta) + B_Y(r)$$

where

B_G is the field produced by the main coils (air core field);

B_S is the field produced by the sectors and the poles;

B_Y is the field produced by all other iron volumes (mostly the yoke) and henceforth indicated as yoke contribution.

It is assumed that the yoke field contribution has cylindrical symmetry since the volumes of iron removed for either the radial penetrations (beam entry and exit, deflectors and magnetic channel feedthroughs) or the axial penetrations (coil supports, cryostat feedthroughs, RF holes), are relatively small compared to the total volume of the yoke and in any case too far away from the midplane to give a significant azimuthal component.

The azimuthal field modulation depends therefore on the pole tips geometry and on the holes drilled through the poles and is in principle dependent on the main coil excitation. However the poles and the pole tips are practically saturated through the operating range of the machine and their contribution can therefore be calculated using the uniform saturation approximation.

The yoke field contribution is calculated with the code POISSON with a model which reduces the actual tridimensional iron structure to a bidimensional one through the use of a reduced permeability value (see Section 3.3). The validity of this approach was tested in the MSU K500 cyclotron and the agreement with the measured data found quite satisfactory both for the field level and for the azimuthal field modulation[10].

3. 2. - Field modulation

The field produced by the poles and the pole tips is calculated assuming an uniform saturation in the z direction with the following values for the magnetization:

poles	$\mu_o M = 21.3$ Kgauss,
pole tips	$\mu_o M = 21.3$ Kgauss,
hills radial part	$\mu_o M = 21.25$ Kgauss,
vacuum chamber inner wall	$\mu_o M = 20.90$ Kgauss.

These values come from the magnetization curves[3] of the different iron casts used for the magnet. Note that the vacuum chamber inner wall is a common C10 iron since its mechanical characteristics are more important than the magnetic ones.

With the above assumptions the field was computed using the current sheet model for the magnetized iron as described in ref. (11). The amplitude of the main harmonics of the field as a function of the radius are plotted in Fig. 13. The peak value of the third harmonic C_3 is in excess of 8 Kgauss around R = 70 cm and in the extraction region it drops to about 7 Kgauss. The amplitudes of the other two harmonics, namely C_6 and C_9, are quite lower. The peak of C_9 around R = 86 cm is due to the radial shape of the sector in that region and to the valley skirt.

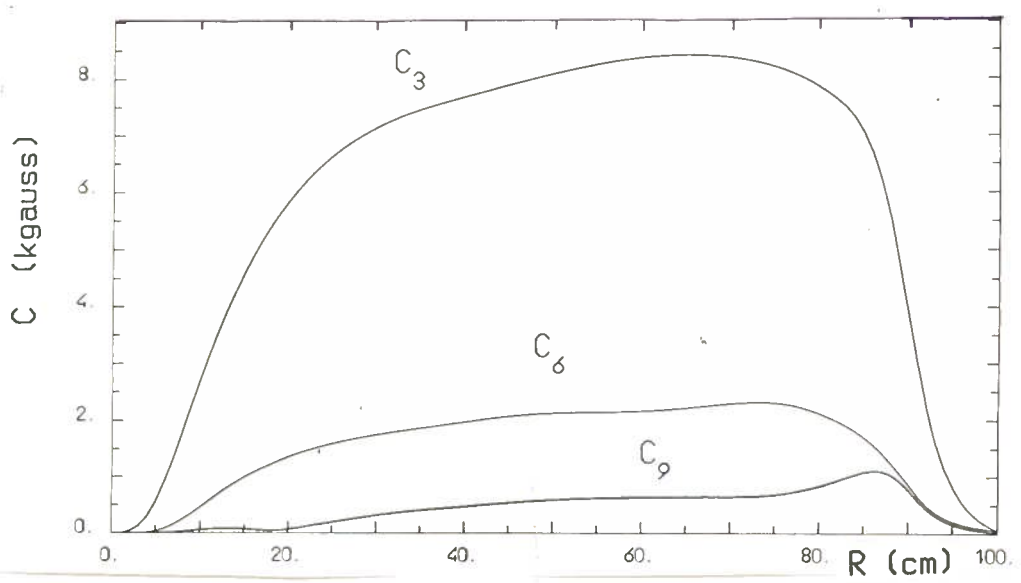

FIG. 13 - Main harmonics of the azimuthal field modulation.

The minimum and maximum azimuthal field values (average field subtracted) are compared in Fig. 14 with the main harmonic C_3. The difference between hill and valley

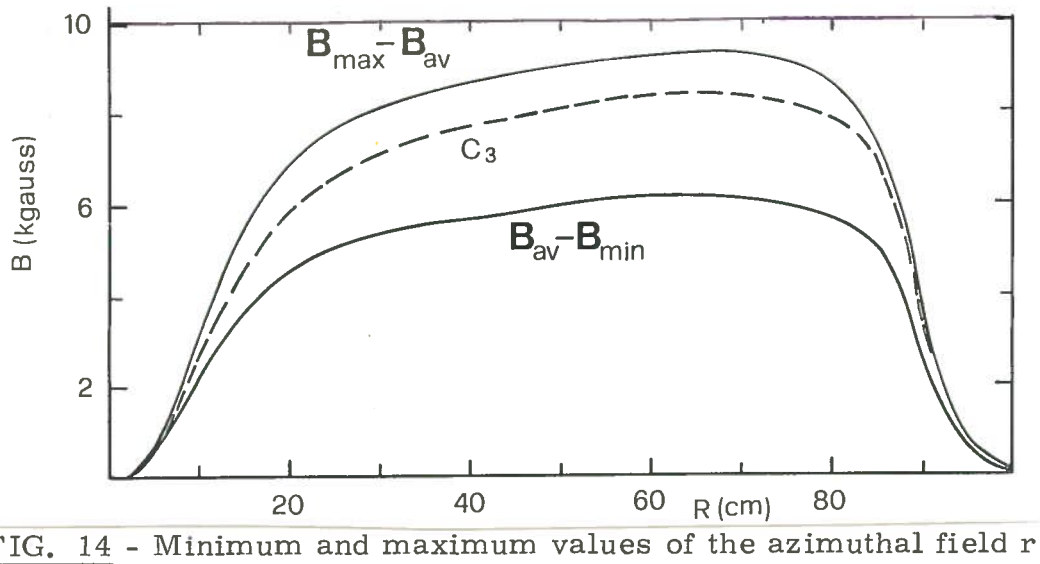

FIG. 14 - Minimum and maximum values of the azimuthal field respect to the average field. Main harmonic C_3 of the modulation is also shown.

fields reaches a peak value of 15 Kgauss in the region between R = 40 cm and R = 80 cm. The asymmetry of the harmonic curve, with respect to the min-max field curve, mostly reflects the difference between the hill and valley widths i. e. 46^{o}-52^{o} versus 74^{o}-68^{o}.

The geometric spiral line, defined as the azimuthal position of the hill center line, and the magnetic spiral line, i. e. the phase of the main harmonic of the field modulation, are plotted as a function of the radius in Fig. 15.

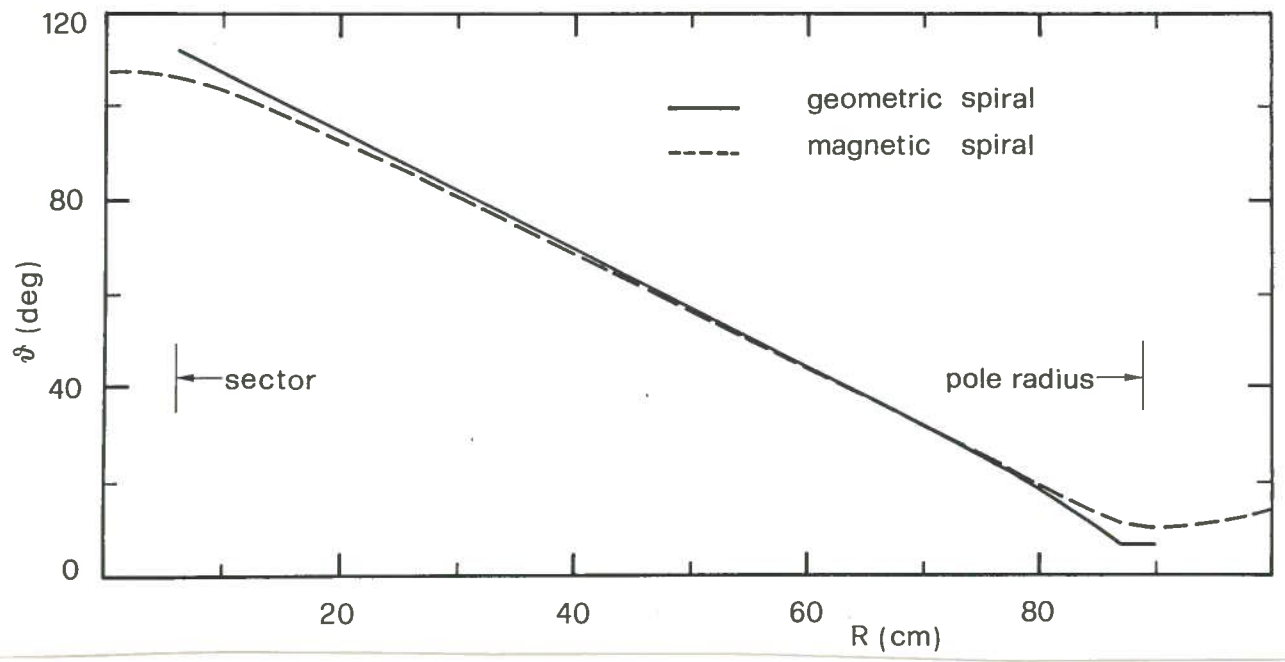

FIG. 15 - Spiral angle of the sector compared with magnetic spiral angle.

The closeness of the two curves, up to R = 80 cm, shows that the magnetic spiral depends mostly on the hill shape with negligible effects from either the valley shims or the holes drilled in the poles. Differences exist in the central region but they are not relevant since there the spiral focusing is negligible. The two curves are instead quite different near the extraction region because of the radial shape of the sectors (R = 86.7--90 cm) and of the valley skirt (R = 87.5-90 cm).

The differences between the geometric and magnetic spiral can be better appreciated by considering the respective spiral focusing terms $tg\,\gamma = k_s r$ (k_s is the spiral constant) which are presented in Fig. 16. At R = 81 cm, where the axial focusing frequency reaches the minimum values, the magnetic spiral focusing term is 20% lower than the corresponding geometric term. This discrepancy points out that in the extraction region, where the axial focusing, the isochronism and the fringing field fall-off play simoultaneously a role in limiting the machine performances, a satisfactory design of the sector geometry can be reached, quite painstakingly, only by trial and error.

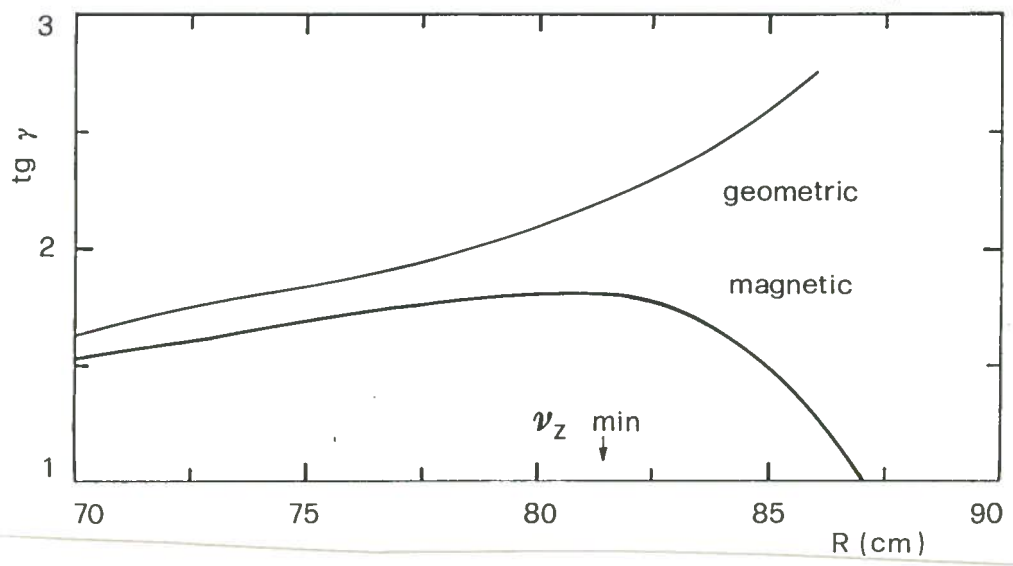

FIG. 16 - Focusing term tg γ as deduced by the geometric and the magnetic spiral angles.

The focusing constant is in excess of $K_{FOC} = 200$ since the minimum axial focusing frequency for fully stripped ions at 100 Mev/n final energy, is $\nu_z = 0.18$ (see Sect. 5). A large safety margin is therefore provided since focusing frequencies of the order of $\nu_z = 0.10$ are usually deemed sufficient.

3. 3. - Average field produced by the iron

The average field produced by the iron is plotted in Fig. 17 at four main coils excitations covering the entire fields range of the machine (B_o = 22-48 Kgauss).

The field level variation is of the order of 3 Kgauss and it is almost independent of the radius. The radial slope of the iron field is close to the optimal one as already pointed out in Section 2.3 and shown in Fig. 11.

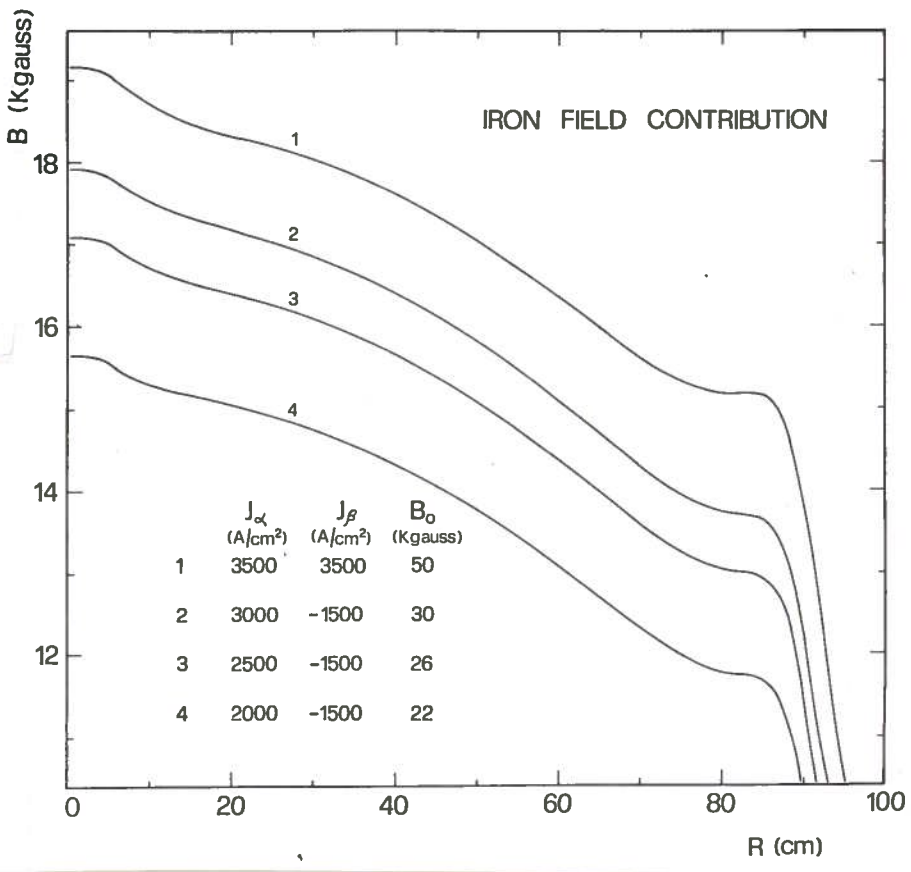

FIG. 17 - Average iron field at four main coils excitations. The values of the total field are also indicated.

The iron average field, according to the model outlined in Section 3.1, is the sum of a constant part, representing the field of the saturated poles and pole tips, and of the yoke field contribution which depends on the main coils excitations. The average field produced by the saturated iron is plotted as a function of the radius in Fig. 18. Also shown are the single contributions of the poles, sectors, and valley shims.

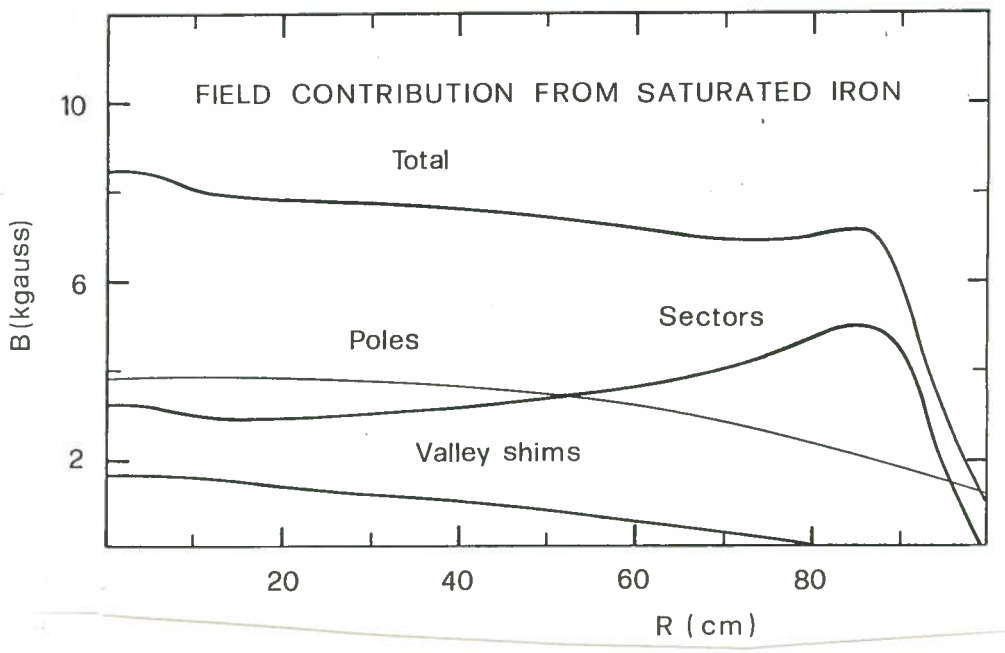

FIG. 18 - Average field contribution from the saturated iron. See text for details.

We recall that the inner tank wall is an integral part of the magnetic structure so that the effective "magnetic" radius of the pole structure is 93 cm against a mecha nical pole radius of 90 cm. The field indicated as pole contribution refers to all the iron volumes located between $z = 45.8$ cm and $z = 90$ cm from the midplane including therefore the solid pole with the central and RF holes and part of the inner tank wall. The field indicated as sectors contribution includes, in addition to the hills, the valley skirt ($R = 87.5$-90 cm) and the inner tank wall up to $z = 45.8$ since they are needed to limit the fringing field fall-off and are therefore an integral part of the sector design.

The valley shims contribution corresponds to the shims placed between $R = 9$ cm and $R = 66$ cm : they provide the optimal radial decrease in the central and mid region of the machine. Pole and sector field contributions are of the same order of magnitude but show a different radial shape. The radial increase of the sector field near the extraction region is balanced by the opposite behaviour of the pole field so that an almost flat field is obtained if one excludes the valley shims contribution.

The sharp fringing field fall-off observed in the total field is due to the increase of the hill width from $\Delta\vartheta = 46^{\circ}$ to $\Delta\vartheta = 52^{\circ}$ in the extraction region and to the presence of the 0.2 mm thick hill shim (see Fig. 6). Visible in the Fig. 18 is also the central

cone field produced by the plug. The cone has a value of ~200 gauss at R = 0 and contributes, together with the 0th coil, some axial focusing in the central region.

The yoke field contribution, as defined in Section 3.1, is presented in Fig. 19 at four main coils excitations corresponding to field levels between 22 Kgauss and 48 Kgauss.

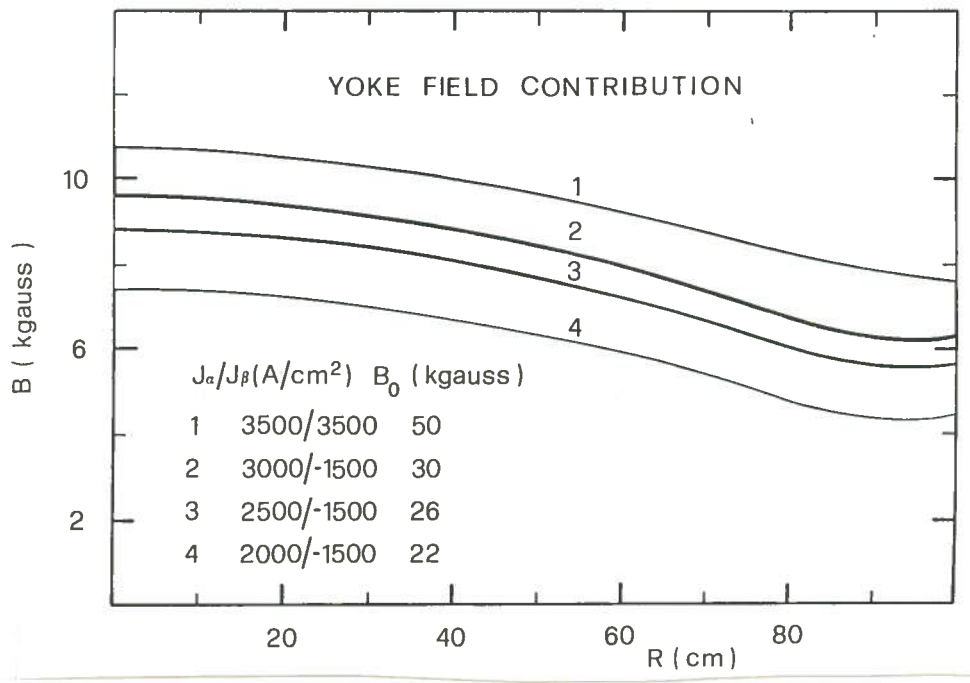

FIG. 19 - Yoke field contribution at four main coils excitations. The values of the total field are also indicated.

The variation of the yoke field level with the main coils excitation reflects the progressive saturation of the iron as shown later. The radial decrease of the field, from the center to the radius of R = 80 cm, is of the order of 2.5 Kgauss and it is practically independent of the field level.

The yoke field is calculated using the program POISSON[12] by reducing the tridimensional structure of the full magnet to a bidimensional one. The parts of the magnet which have circular symmetry, like the coils and the overall yoke structure, are treated exactly. All the elements without cylindrical symmetry, like the sectors, the RF holes, the axial and radial penetrations through the yoke, are replaced by cylindrical iron rings with a magnetization law given by:

$$B = \mu_o(H + F\,M)$$

where the fraction F is the ratio between the actual iron volume of the elements and the volume of the rings.

The iron fractions used for the different regions are indicated on the relaxation grid of Fig. 20 which shows how the magnet is represented for the POISSON calculations.

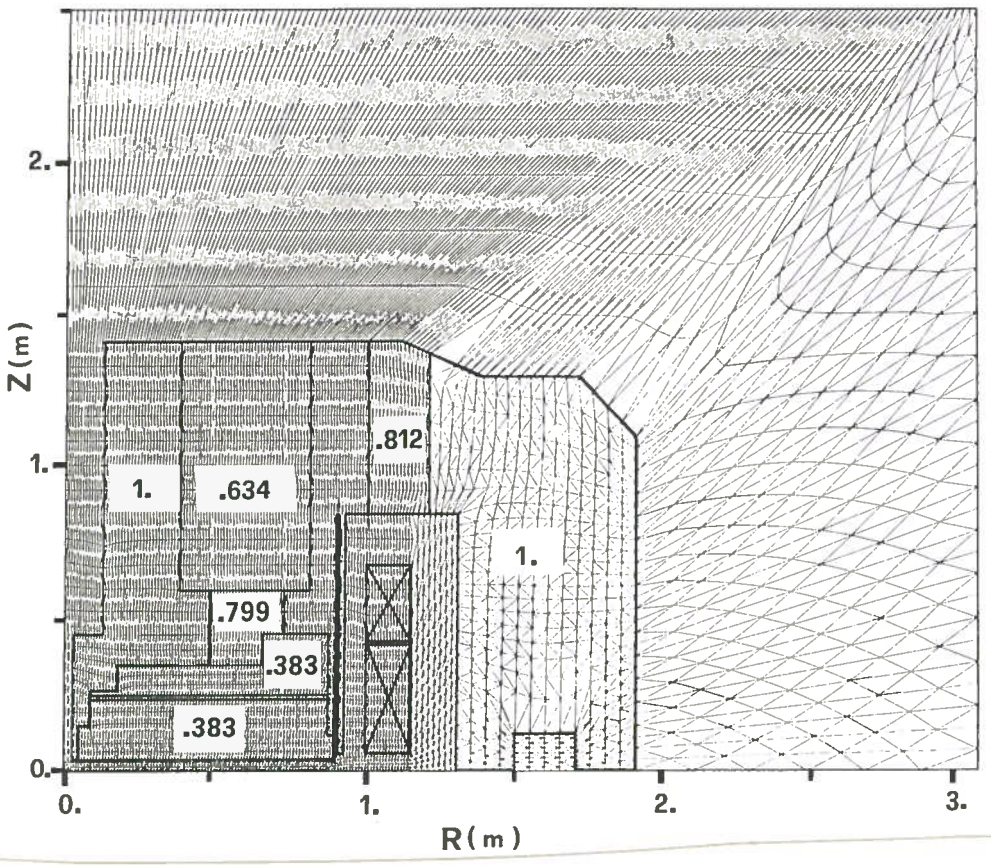

FIG. 20 - POISSON relaxation grid used for the magnetic field calculation. The iron fractions of the different regions are indicated. See text for details.

The yoke field is obtained by subtracting from the total field at the midplane the air-core field of the main coils and the pole and pole tips field contributions. The latter are calculated, assuming an uniform saturation in the z direction, according to the schematization used for the POISSON grid, i. e. rings with variable magnetization values.

POISSON calculations were carried out at 28 main coils excitations covering the operating range of the machine in the (I_α, I_β) plane. The POISSON grid on the (I_α, I_β) plane was selected so as to obtain a precise and reliable interpolation scheme for the trimming field calculations (see Section 4).

The average iron field contribution at R = 80 cm, as calculated by the POISSON code, is presented in Fig. 21 as a function of the total field. Positive or negative excitation of the β section is indicated and a line is traced to show the overall trend.

The progressive saturation of the yoke at increasing main coils excitations is visible. The iron field contribution to the total field is approximately 50% at the low excitations and decreases down to 30% at the maximum field level.

The field in the yoke holes corresponding to the beam entry and exit paths is also evaluated with the POISSON program. All the midplane yoke holes are simulated by a cilindrical iron free ring, enclosed in the yoke (see Fig. 20), with an height of 25 cm

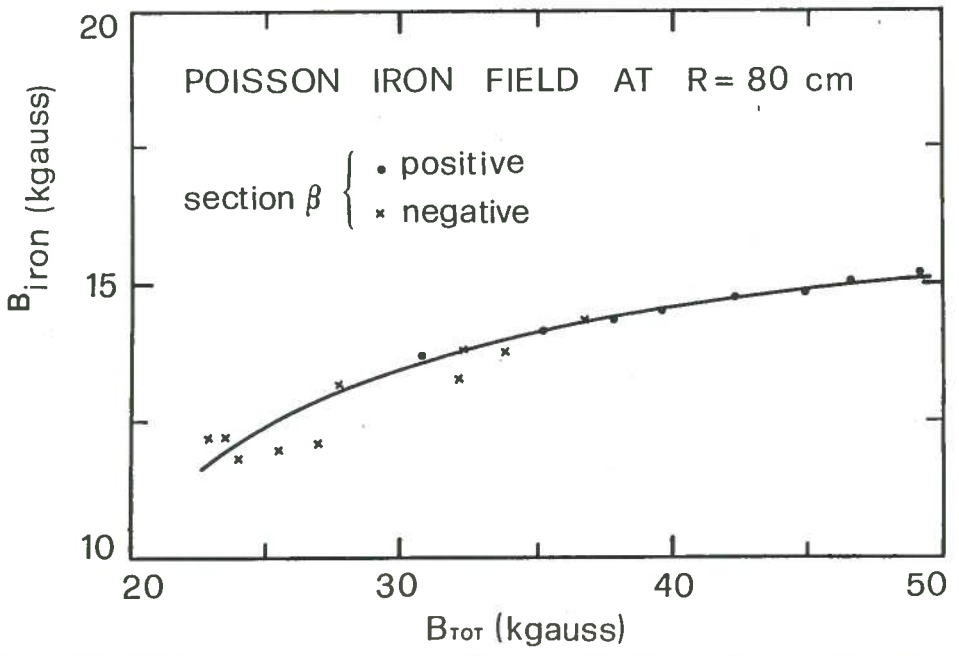

FIG. 21 - Average iron field contribution at R = 80 cm, as calculated by the POISSON code, as a function of the total average field at the same radius. Positive or negative excitation of the coil β section is indicated.

and an equivalent volume. The beam entry and exit holes have a cross section of 25x25 cm^2 and therefore the computed field should be quite close to the actual value.

The yoke hole field is presented in Fig. 22 as a function of the total field at R = = 80 cm in order to correlate its value to the operating diagram of the machine.

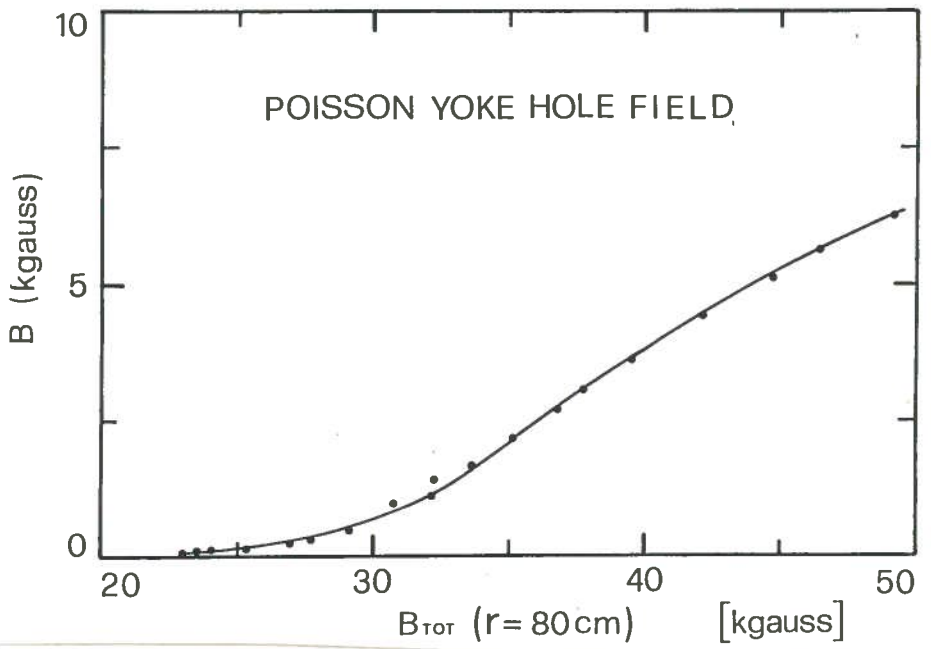

FIG. 22 - Yoke hole field, as calculated by the POISSON code, vs the total average field at R = 80 cm.

At the lowest excitations, i. e. for total field values below 30 Kgauss, the field in the holes is practically zero as expected since the yoke iron is far away from satu

ration. The field increases, almost linearly, with the excitation reaching the value of 6 Kgauss at the maximum field level.

The beam entry and exit paths are therefore influenced by these fields values which have been taken into account in the injection and in the extraction studies.

Accuracy of these field values is not critical so that the possible errors of the POISSON code, estimated to be in the range 10-20% for the yoke hole field calculation, will not affect the design of the injection and extraction process.

4. - TRIMMING OF THE MAGNETIC FIELD

4.1. - Computing methods

The magnetic field of the cyclotron is represented by a magnetic field map with a radial step of 1 cm from R = 0 to R = 130 cm and an azimuthal step of 1^{o} over a 120^{o} sector.

The map is obtained by the superposition of a total radial average field and a modulation map (i. e. a map with zero azimuthally averaged field). The modulation map is constant being produced by the saturated pole tips.

The total radial average field is obtained by fitting the "isochronous field", $B_{IS}(r)$, analytically calculated or externally supplied, using as parameters the excitation of the two main coil sections and of the twenty trim coils. The main coils and trim coils air-core fields and the iron field were presented in Sections 1 and 3.

The fitting is done via a standard least squares procedure i. e. setting between r_1 and r_2

$$\Sigma\left[w(r)\left(B_{IS}(r) - B_{IRON}(r) - I_{\alpha}F_{\alpha}(r) - I_{\beta}F_{\beta}(r) - \sum_{K} I_K F_K(r)\right)^2\right] = \min$$

where

$B_{IS}(r)$	is the isochronous field for the given ion;
$B_{IRON}(r, I_{\alpha}, I_{\beta})$	is the iron field contribution;
$F_{\alpha}(r)$, $F_{\beta}(r)$, $F_K(r)$	are the form factors of the two main coils section and of the kth trim coil;
I_{α}, I_{β}, I_K	are the currents of the two main coils sections and of the kth trim coil;
r_1, r_2	are the initial and final fitting radii;
$w(r)$	is a weight function.

The isochronous field $B_{IS}(r)$ when calculated by the code itself is specified by giving the charge to mass ratio Z/A of the ion considered and the nominal center field

value B_o which defines the RF accelerating frequency as $\omega_{RF} = hB_oZ/A$ (h is the harmonic number). The isochronous field is calculated by an iterative procedure[13] using the harmonic of the modulation map up to the order 5N where N is the sector number. A "quasi-isochronous field" can also be generated by specifying over a radial interval an isochronism error function $\Delta\tau/\tau$. The procedure automatically computes a field and produces the specified isochronism error. This feature is routinely employed for the following reasons:

a) to compensate the errors produced by the analitycal formula for the isochronous field;

b) to deisochronize the field near the extraction region in order to balance the phase curve and/or to control the axial focusing;

c) to produce a cone field in the central region in order to assure some magnetic focusing.

The fit is normally imposed between R = 3 and R = 84 cm with a weight function $w(r) = (r/r_2)^2$ i. e. proportional to the radial turn density. Since the $B_{IRON}(r)$ is a function of the (I_α, I_β) main coil currents an iterative procedure is followed in the fitting.

An initial fitting is done by using a guessed value of (I_α, I_β). Afterward the $B_{IRON}(r)$ is recalculated using the (I_α, I_β) given by the fit and the procedure is repeated until the two successive values of (I_α, I_β) are less than a specified value (tipically 0.1 A). The procedure normally converges in 4-5 iterations independently of the initial guess. At low excitations where the iron field is more sensitive to the current variations the convergence is slower and requires 9-10 iterations.

The calculation of $B_{IRON}(I_\alpha, I_\beta, r)$ is done by fitting a third order polynomial in (I_α, I_β) over the 16 points, out of the 28 available as indicated in Fig. 23, closer to the desired point in (I_α, I_β) plane.

The fitting can be done either with all the trim coil currents free or setting upper limits on their individual values or on the max trim coils power. The 0th coil, which produces the central cone field, can be used or not. Once the values of the main coils and of the trim coils currents are found a total average field is generated between $0 < R < 130$ cm and summed to the iron modulation map to produce the magnetic field map. The validity of the calculated settings is tested with the E. O. code which yields the phase slip curve and the focusing frequencies ν_r, ν_z. The results of the E. O. runs are reported in Section 5.

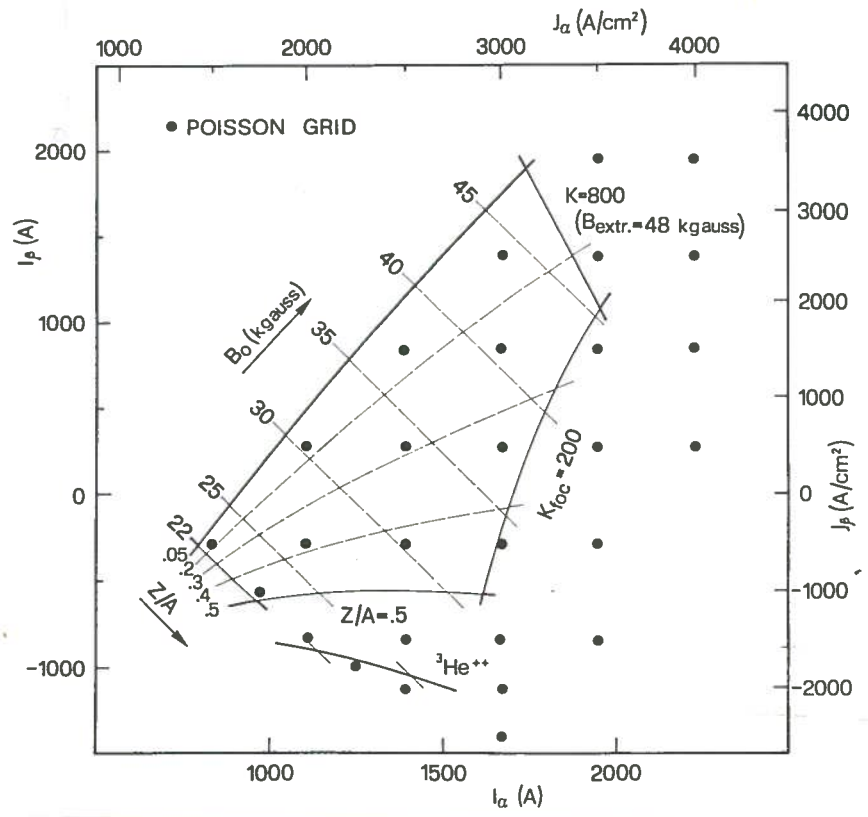

FIG. 23 - Operating diagram of the cyclotron in the (I_α, I_β) plane. The dots mark the excitation values used for the POISSON calculation.

4. 2. - Cyclotron current settings

The operating diagram of the machine in the plane (I_α, I_β), obtained with the trimming procedure described in the previous Section, was presented in Fig. 23.

The main coils require current densities between 1000÷3500 A/cm^2 for the section and - 2000÷+3500 A/cm^2 for the β section. Negative currents in the β section are therefore required for low field values i. e. below 35 Kgauss. The trim coil power is fairly low and is presented in Fig. 24 interms of equipower lines on the operating diagram of the machine. Values of the power for selected

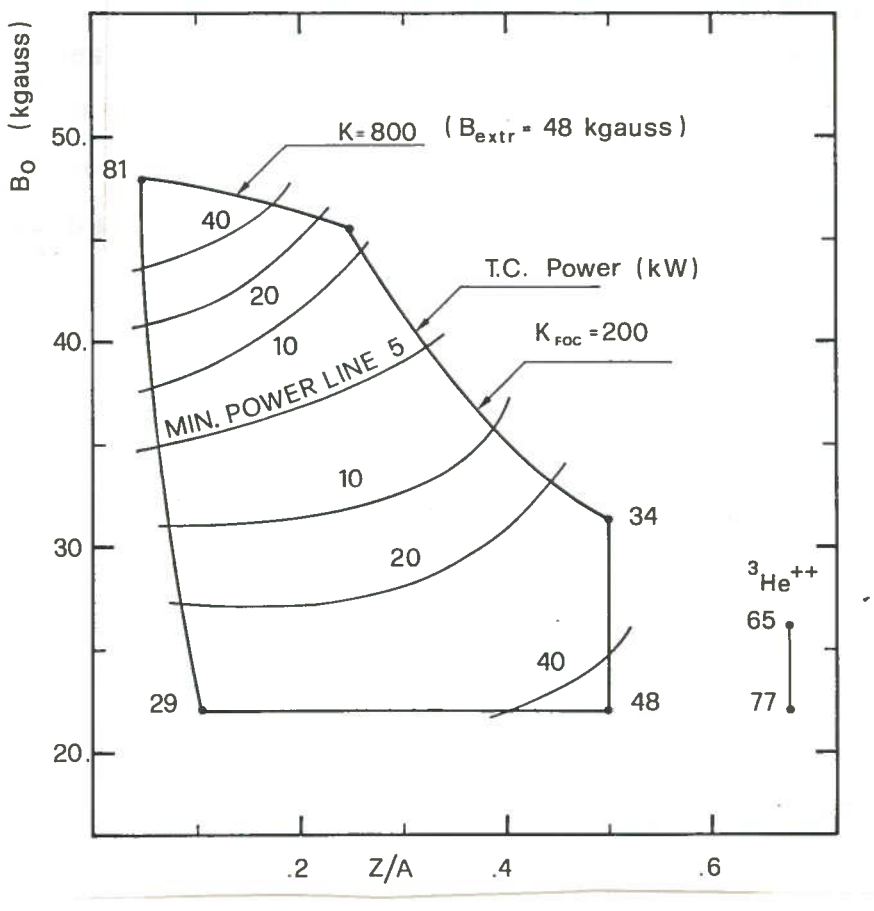

FIG. 24 - Trim coils equipower lines for the operating diagram of the cyclotron. Power values are indicated for selected ions.

ions along the contour of the diagram are indicated. The line of minimum power is also plotted: the value of 5 kW, as opposed to the theoretical zero value, reflects the differences between the actual iron field and the B_{best} field. Note that the calculated power does not include trim coil leads and power supplies losses in order to reflect more directly the difficulties of the field isochronisation.

The power requirements, as apparent from Fig. 24, look well balanced since the highest power is needed at the corners of the operating diagram as expected from the optimization process outlined in Section 2.3. The trim coils current pattern and their field contributions vary considerably over the operating range and are antisymmetric with respect to the minimum power line. Examples for selected ions are presented in Figs. 25 and 26 for limiting cases both in terms of the trim coils power and the field contribution.

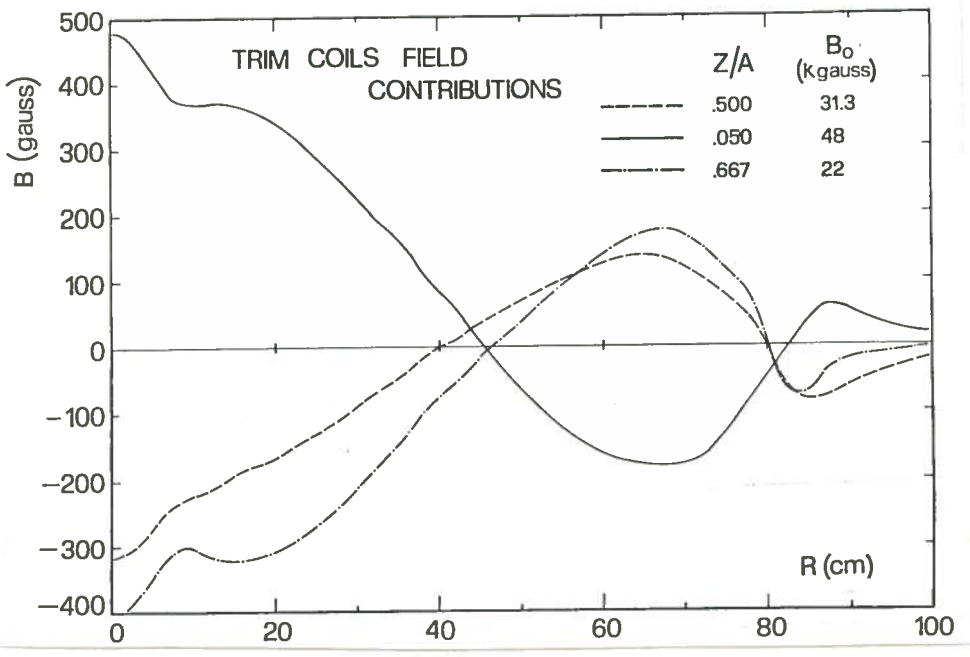

FIG. 25 - Trim coils field contributions for the isochronization of the indicated ions.

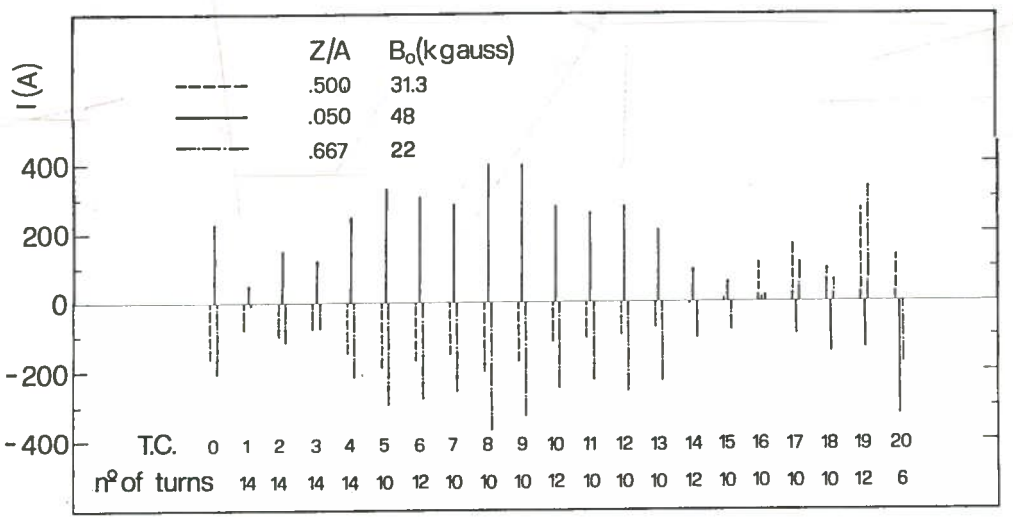

FIG. 26 - Trim coils currents setting for the indicated ions.

Maximum currents in the trim coils are limited to 400 Amps corresponding to an excitation of 4000 At (2000 At for TC-20). These values are reached in the high power cases but without prejudice for the beam dynamics as seen in the next Section.

5. - EQUILIBRIUM ORBIT PROPERTIES AND BEAM DYNAMICS

5.1. - General features

The validity for beam acceleration of the computed fields is tested with the Equilibrium Orbit code which provides the phase curve and the focusing frequencies. The main constraints placed on the isochronous field are

- A cone field in the central region able to provide an axial magnetic focusing $\nu_z > 0.1$ for $R > 7$-8 cm and an appropriate starting phase for the beam so as to assure axial electric focusing. This starting phase is set at 25^o at the second turn for the E. O. run, a value consistent with the central region design[14].
- A minimum value of the axial focusing frequency around the extraction region of $\nu_z > 0.1$ obtained, if necessary, by local deisochronisation of the field.
- A balanced phase curve i. e. zero over most the accelerating cycle and oscillating between $\pm \varphi_{max}$ in the extraction region, where φ_{max} is the phase value at the deflector entrance.

For each ion the appropriate harmonic number for the RF system is chosen and the peak dee voltage, of constant value at all radii, is scaled to obtain a constant orbit mode acceleration. The number of turns, the min and max peak dee voltages and the min and max energies for each harmonic mode are given in Table VI.

TABLE VI - Number of turns and peak dee voltage for different harmonic modes.

h	Nt	V_{dee} (kV)	T/A (MeV/n)
1	700	40-100	35 -100
2	350	22- 93	8.5- 35
3	220	22- 71	3.7- 8.5
4	150	22- 63	2.5- 3.7

These values were derived from the central region studies for the h = 1, 2 mode and roughly scaled in the other two cases.

5. 2. - Equilibrium orbit properties

The phase curve and focusing frequencies ν_r and ν_z are presented, as a function of radius, together with the average total field in Figs. 27, 28, 29 and 30 for eight representative ions lying on the contours of the operating diagram. They correspond, for any given charge to mass ratio, to the minimum and maximum operating field.

The Helium 3 beam at the minimum field of 22 Kgauss corresponding to a final energy of 80 Mev/n and at the max field of 26.2 Kgauss corresponding to 130 Mev/n is presented in Fig. 27.

Visible in the figure are the cone field in the central region and the corresponding phase slip. The field has a very good isochronism over most of the accelerating cycle with a peak phase value of $\pm 35^{o}$ near extraction.

The minimum axial focusing frequency, for the high energy case, is close to $\nu_z = 0.2$ i. e. with a comfortable margin over the minimum allowed value $\nu_z = 0.1$. At the low field (22 Kgauss) the increase of the flutter determines an axial focusing frequency of $\nu_z = 0.5$ near R = 70 cm.

The very sharp increase of the ν_z value at extraction is consequent of the fringing field fall-off and is limited by the radial cut of the hill profile.

The oscillations visible in the axial focusing curve are generated by the trim coils and correspond to small field gradients above and below isochronism. The oscillations are more marked for the high field case which is also an high power case. Correspondingly the fit to the isochronous field, even though good, is not as good as in the low field case.

The same curves for the fully stripped light ion at the minimum and maximum final energies of 44 and 100 Mev/n are presented in Fig. 28. The phase curve and the axial frequency curve are quite similar to the previous case with a minimum $\nu_z = 0.2$ and phase $\varphi = \pm 35^{o}$ for the high energy case. Note that the oscillations in the ν_z curve are much reduced since the trim coil power is also reduced (see Section 4). For the low energy case the ν_z is very high, reaching near extraction values in excess of 0.7. Problems can be expected because of resonances as seen in the next paragraph.

A similar behaviour occurs in the two other cases i. e. the ions with Z/A = 0.25 and Z/A = 0.16. Note that the case Z/A = 0.25 and $B_o = 45.5$ corresponds to the intersection of the focusing and the bending lines while the case 0.16/47 lies on the bending line.

The ensemble of this results show that :

- a minimum axial focusing frequency $\nu_z > 0.1$ is assured in the central region while $\nu_z > 0.2$ is assured near extraction;

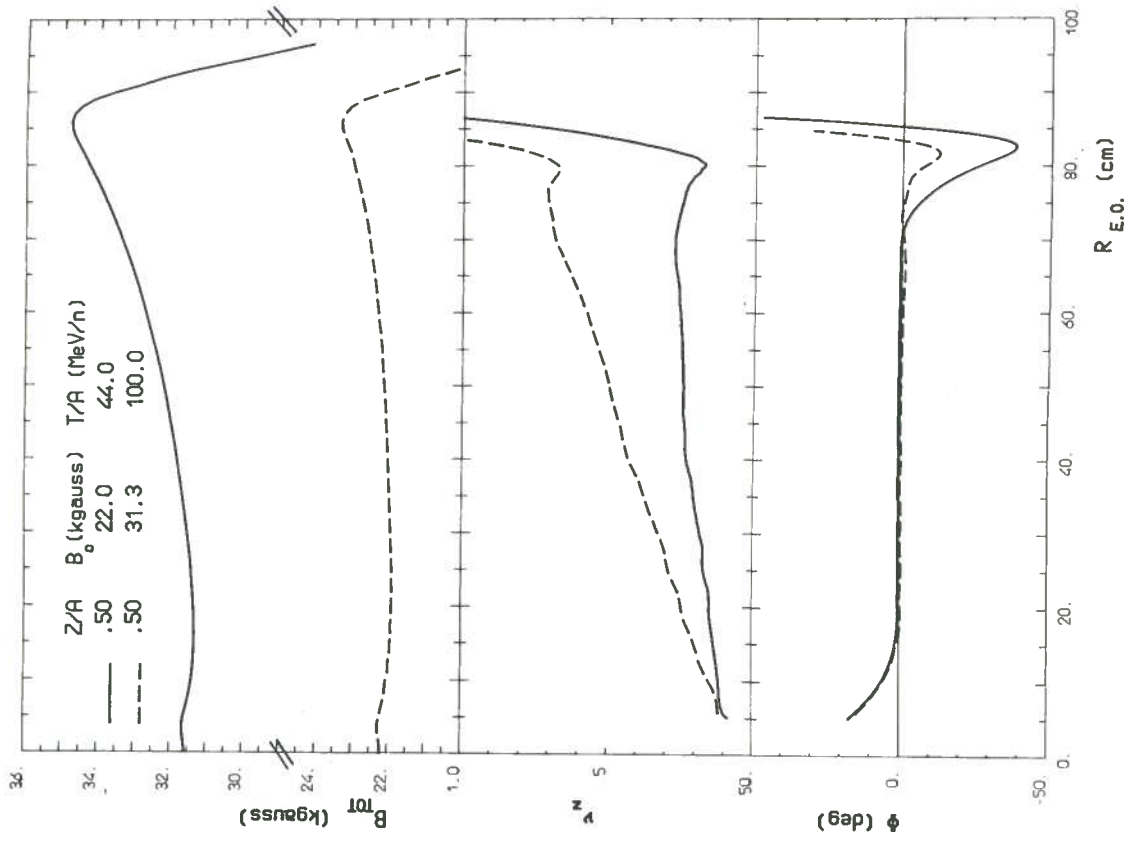

FIG. 28 - Average total field, axial focusing frequency and phase for the indicated ions.

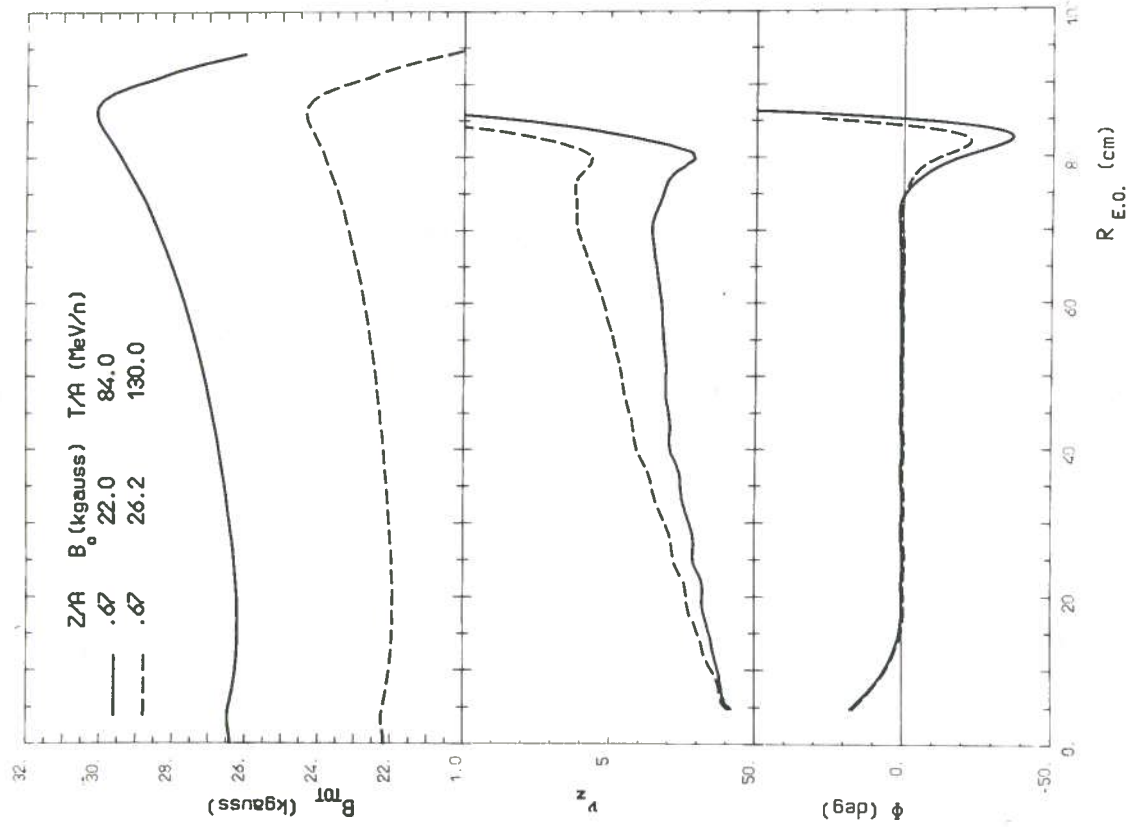

FIG. 27 - Average total field, axial focusing frequency and phase for the indicated ions.

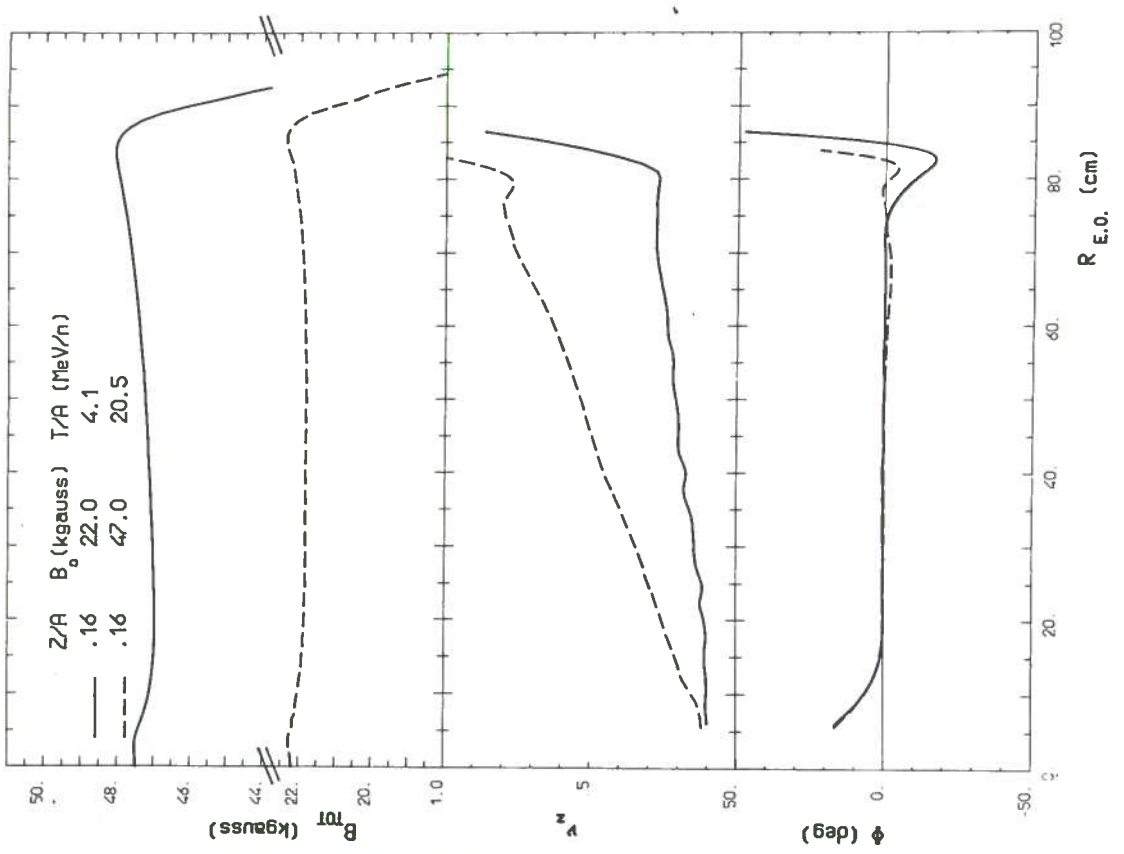

FIG. 30 - Average total field, axial focusing frequency and phase for the indicated ions.

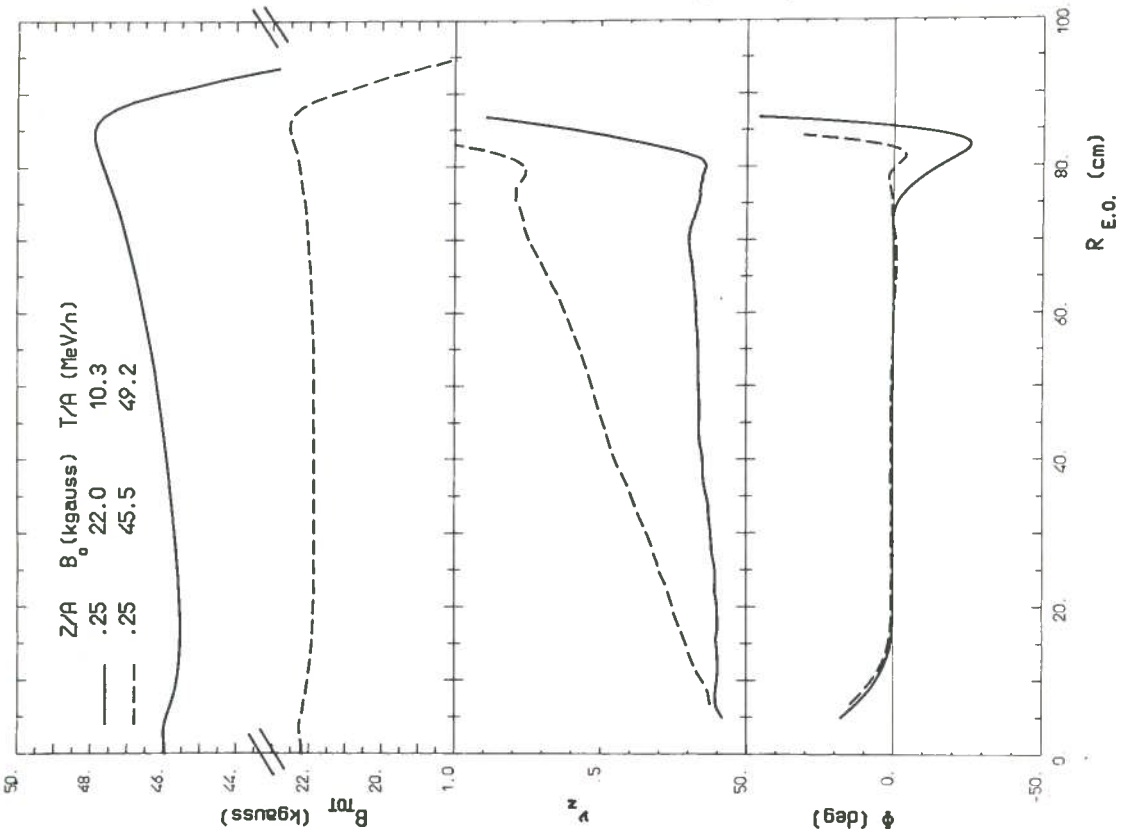

FIG. 29 - Average total field, axial focusing frequency and phase for the indicated ions.

- the cone field provides the right starting phase for some axial focusing in the central region (R < 5 cm);
- the phase curve is well centered around the zero value for the acceleration cycle with exclusion of the extraction region;
- the phase curve is nevertheless well balanced at extraction between $\pm\varphi_{max}$; the max values are of the order of 35 deg along the focusing line i. e. for the maximum turn number (h = 1).

5. 3. - Beam dynamics

The working path in the (ν_r, ν_z) plane for three ions, which are representative of the general behavior, is shown in Fig. 31 where major resonance lines are plotted. Examination of the curves show that the extraction, via the excitation of the $\nu_r = 1$ resonance with a first harmonic in the magnetic field, takes place in proximity of the $\nu_r + 2\nu_z = 3$ resonance. The lower the magnetic field the closer the extraction to the resonance. The resonace $\nu_r + 2\nu_z = 3$ is an essential resonance since does not depend on imperfections of the magnetic field. This resonance couples the radial to the axial motion and since it is a sum resonance the axial growth of the beam is not limited. The beam approaches the resonance with an intrinsic radial oscillation (produced by the excitation of the $\nu_r = 1$ resonance) and therefore a fast increase with the turn number of the axial beam height is observed[15]. This resonance cannot be crossed and therefore the extraction must take place before the resonance.

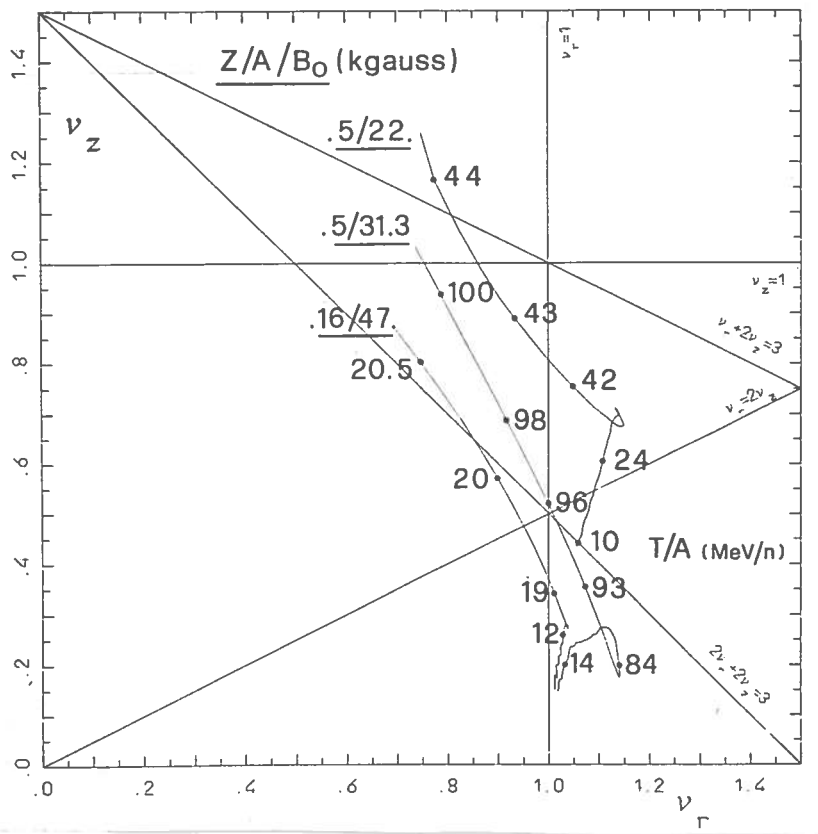

FIG. 31 - Working path in the (ν_r, ν_z) plane for three typical ions.

For low fields the resonance is approached at progressively higher values of ν_r imposing a limit (22 Kgauss) on the minimum field value compatible with the beam extraction. The field limit $B_o = 22$ Kgauss must thus be regarded as the lowest one com-

patible with a beam extraction and a tolerable beam blow-up.

A second dangerous resonance is the $\nu_r - 2\nu_z = 0$ (Walkinshaw resonance) which for the higher fields is crossed after the $\nu_r = 1$ resonance. The beam has therefore a radial oscillation which induces an axial beam blow-up when crossing the resonance itself[15]. The behaviour of the radial focusing frequency ν_r and of $\nu_r + 2\nu_z$ for three ions in the extraction region are plotted in Fig. 32 as a function of the average radius

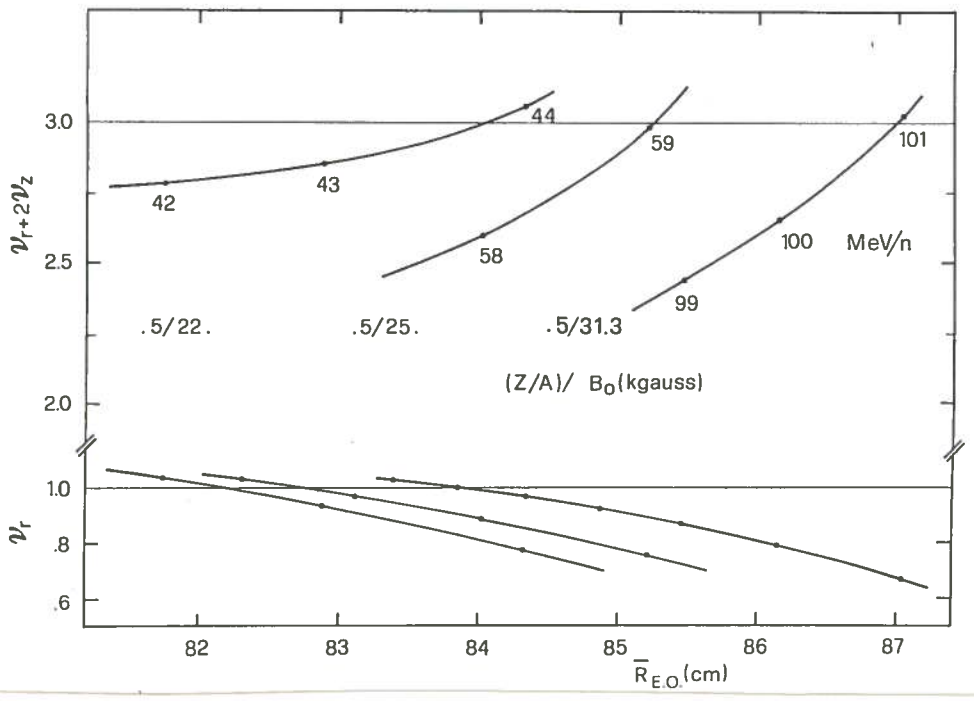

FIG. 32 - $(\nu_r + 2\nu_z)$ and ν_r values for the fully stripped ions at the indicated field levels as a function of the radius.

of the E. O. The three ions considered span the widest range in terms of resonance approach. The extraction of the ion 0.5/31.3, which is the most difficult one to extract, takes place at $\nu_r = 0.76$ i. e. 100 Mev/n. The onset of the $\nu_r + 2\nu_z = 3$ resonance forces the extraction of the ions accelerated at lower fields at progressively higher ν_r values, which reach 0.85 in the case of the $B_o = 22$ Kgauss level.

Overall it is found that the extractor must move over the radial range R = 83,5--86.3 cm and for this reason the last trim coil, located between R = 83-86.7 has only one layer. More details on the extraction system can be found in ref. (8).

6. - INFLUENCE OF THE TRIM COILS FIELD MODULATION

The excitation of the trim coils in the trimming operation mode (i. e. equal current in all the three windings which make up one trim coil) produces, in addition to the average field needed for fitting the isochronous field, an azimuthal field modulation with harmonic content n = 3, 6, 9 etc since the trim coils windings have a three-

-fold symmetry.

The average field and the harmonics C_3 and C_6 produced by the excitation at 3000 At of two typical trim coils, the N. 7 with average radius R = 34.5 cm and the N. 16 with R = 68.7 cm, are presented as a function of radius in Fig. 33. We recall that the maximum excitation anticipated in the trimming mode is 4000 At (See Section 2).

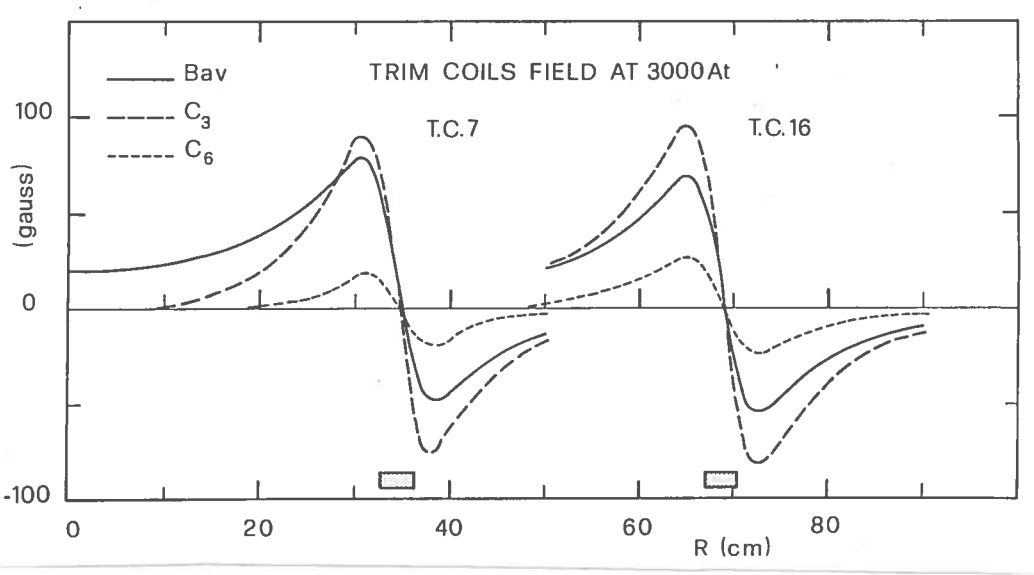

FIG. 33 - Average field and harmonics C_3 and C_6 of two trim coils at the excitation of 3000 At.

As visible in the figure the positive excitation of the trim coils adds a modulation to the field at inner radii and subtracts it at outer radii (inner and outer are referred to the T. C. average radius). The harmonic C_3 of the modulation has a maximum absolute value of the order of 100 gauss close to the T. C. radius while the harmonic C_6 is a factor 5 lower.

The field modulation produced by the trim coils changes the isochronous field and the focusing frequencies ν_r and ν_z. In fact all these quantities are a function of the harmonics and their derivatives and the total field modulation must therefore be taken into account in the isochronization procedure. Changes in the current settings of the main coils and of the T. C. with respect to the values calculated in Section 5 are therefore anticipated.

The trim coils field modulation is however essentially a perturbative effect and correspondingly it was not considered in the previous sections where the emphasis was on the design features of the magnetic field.

The contribution of the trim coils to the harmonics of the modulation field $C_N(r)$ and to the isochronous field $B_{IS}(r)$ can be calculated, in a linear approximation as:

$$\Delta C_N(r) = \sum_K (AA_K + BB_K) I_K$$

$$\Delta B_{IS}(r) = - \frac{1}{2(N^2 - 1)} \frac{1}{B_{rel}(r)} \sum_K \left[2(AA_K + BB_K) + r \frac{d}{dr} (AA_K + BB_K) \right] I_K$$

where

N	is the sector number;
B_{rel}	is the relativistic field for the ion considered;
A, B	are the Fourier components of order N of the main field modulation;
A_K, B_K	are the Fourier components of order N for a unit current excitation of the kth trim coil;
I_K	is the current excitation of the kth trim coil.

Only the harmonic of order N is considered but the formula can be extended to any desired order.

The contribution to the isochronous field coming from the T. C. produced modulation is calculated by inserting the above formulas in the least squares fitting procedure.

The field obtained is consistent in the sense that the calculated main coils and trim coil currents fit the isochronous field corresponding to the modulation produced by the iron pole tips and by the trim coils themselves. A final field map is therefore obtained by adding to the total average field both the iron modulation map and the modulation produced by the trim coils at their calculated currents. The validity of the procedure has been extablished by running the equilibrium orbit code on the final map. No significant phase slip error with respect to the unperturbed case has been detected. According to the above formulas the T. C. produced modulation is practically negligible at high field levels and plays some role only at low field levels and high trim coils currents i. e. in first approximation, high trim coil powers.

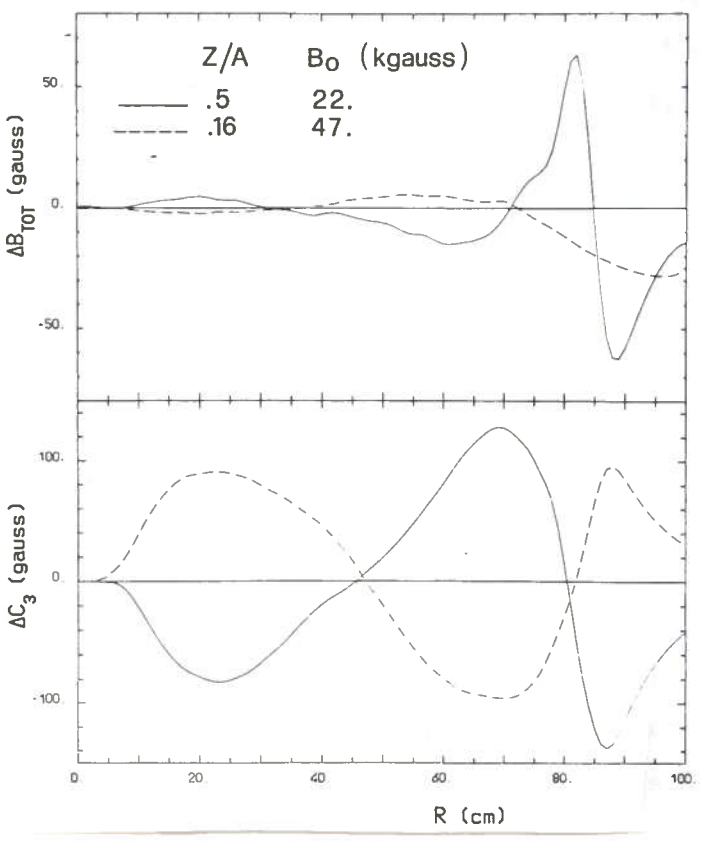

FIG. 34 - Perturbation on the 3rd harmonic (ΔC_3) and on the isochronous field (ΔB_{TOT}) produced by the trim coils for the indicated ions.

The contributions of the T. C. produced modulation to the main field harmonic C_3 and to the isochronous field B_{TOT} are presented for two ions in Fig. 34. These ions have been selected since they require a relatively high T. C. power and run respectively at the min and max field levels. For all the ions within the operating diagram the 3rd harmonic variation is less than 120 gauss but it produces indeed isochronous field variations up to 60 gauss for the low field levels, as shown in Fig. 34, near extraction.

Main coils currents are slightly changed with respect to the case when the T. C. produced modulation is not taken into account. Trim coil currents changes are more marked, expecially for the last T. C. group, but are still within the limits set in Section 2 and the T. C. power is practically unaltered. For some low field levels cases it is even reduced by 10%.

In the case of the high field level the pattern of ΔC_3 and ΔB_{TOT} is symmetric with respect to the other case since it reflects the sign change of the trim coil currents (see Section 4.2).

The influence of the T. C. produce modulation on the focusing frequencies ν_r, ν_z is practically negligible for the high field levels. An expanded view of the working path in the ν_r, ν_z plane with and without the T. C. produced modulation is presented in Fig. 35 for the $Z/A = 0.5$ ion at the field of 31.3 Kgauss.

An increase of ν_z is observed between R = 60 cm and R = 80 cm in correspondence of the increase of the main field harmonic.

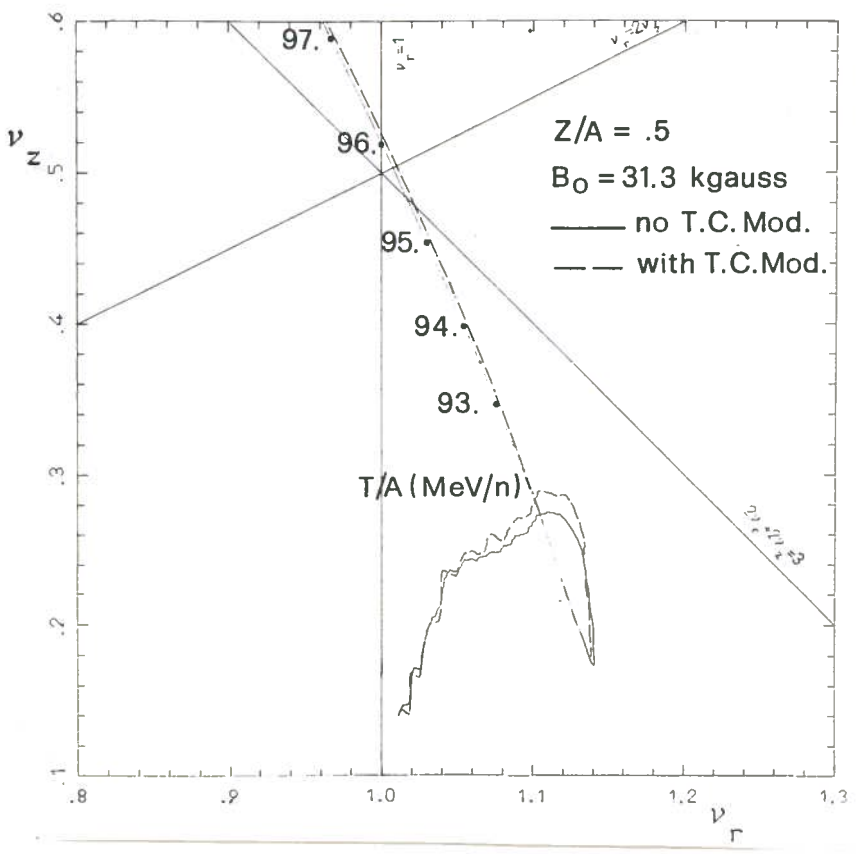

FIG. 35 - Working path in the (ν_r, ν_z) plane for the indicated ion without (solid line) and with (dashed line) the trim coils modulation.

The working path in the extraction region is practically unaltered and therefore no significant modifications of the beam dynamics are foreseen.

The working path for the $Z/A = 0.5$ ion at the field level of 22 Kgauss is presented in Fig. 36. Sensible changes occur expecially in the extraction region. The ν_z values are there sensibly increased so that the entire working path is shifted closer to the resonace line $\nu_r + 2\nu_z = 3$.

This effect is mainly due to the modification of the fringing field region (see Fig. 34) and to

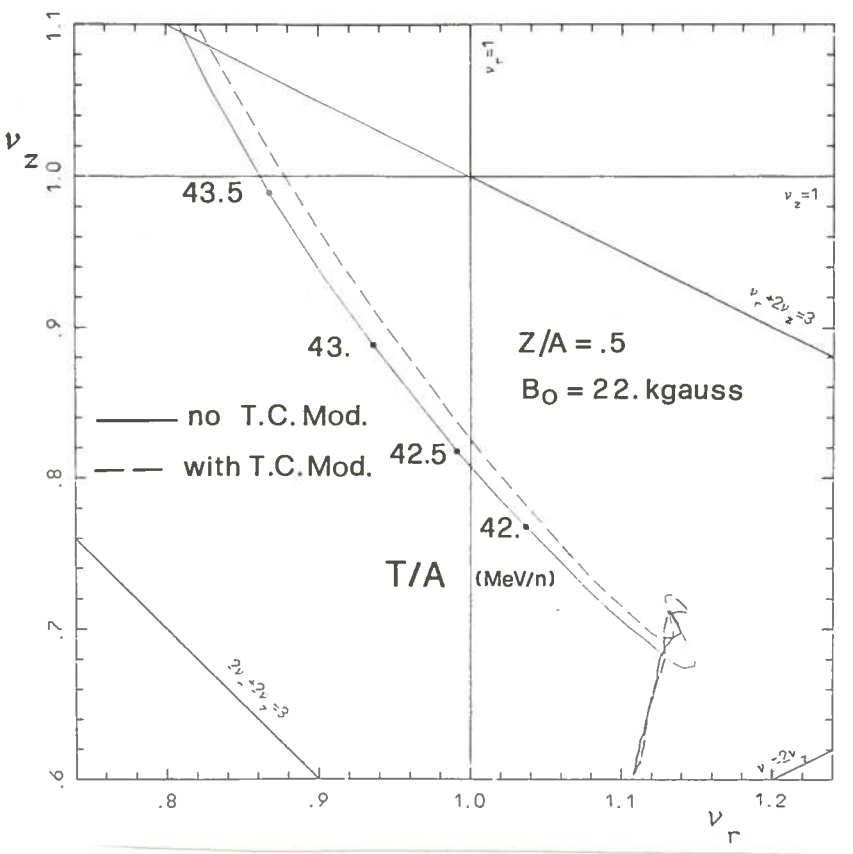

FIG. 36 - Working path in the (ν_r, ν_z) plane for the indicated ion without (solid line) and with (dashed line) the trim coils modulation.

the high scalloping of the equilibrium orbit ($\pm$ 3 cm). These changes however are not critical for the extraction process.

As a conclusion we can say that the T. C. produced modulation can be neglected in the design stage of the machine. Obviously the setting of the cyclotron for beam acceleration does depend on the T. C. produced modulation. At the high field level it may be possible to ignore the T. C. produced modulation by accepting a non optimized phase slip curve. At the low field level instead the phase slip becomes too large (as inferred from the high values of ΔB_{TOT} in Fig. 34 and therefore the beam will not reach the extraction region unless corrections are carried out.

7. - FIRST HARMONIC CONTROL

7. 1. - The harmonic coils

Control of the first harmonic of the magnetic field is essential at extraction (R = = 82-84 cm) since the turn separation of the beam at the deflector entrance is achieved with the excitation of the $\nu_r = 1$ resonance.

First harmonic control is also necessary at the exit of the central region (R = = 10-15 cm) to center properly the beam when it crosses the $\nu_r = 1$ resonance.

The trim coils (1, 2) or (3, 4) and (19, 20) will therefore be operated as harmonic coils in addition to the standard trimming mode. The combined excitation of two adiacent trim coils to form a single harmonic coil has been selected to provide a variable form factor for the first harmonic. Note that, apart from manifacturing and assembly tolerances of the machine components, there will be an intrinsic first harmonic in the magnetic field due to the lack of symmetry (cilindrical of 3-fold) of some components. The main sources of this intrinsic first harmonic (and other additional perturbation) are:

- asymmetries in the main coils due to the turn to turn climbs and to the connection between the pancakes;
- the passive magnetic channels used for the extraction;
- the midplane yoke penetrations for the beam entry and exit ports and for the deflectors and magnetic channels actuators.

Partial compensation can be achieved for the above cases and specifically:

- the pancakes of the main coils will be magnetically centered[16] so that the total first harmonic produced by each coil section will be minimized at R = 83 cm which is the average radial value where the $\nu_r = 1$ resonance occurs;
- the passive magnetic channels are compensated by the moving bars C1A, C1B, C2 which cancel the first harmonic at the $\nu_r = 1$ location and minimize the second harmonic;
- the perturbations to the magnetic field produced near the extraction radius by the holes in the yoke are practically cancelled out by drilling two additional compensating holes in the yoke midplane.

The harmonic coils should therefore offset the residual first harmonic originated by the manufacturing and assembly tolerances and by the partial compensation scheme described above, and provide the amplitude and phase of the first harmonic necessary for beam extraction and for centering. These amplitudes are of the order of 10 gauss and 20 gauss respectively for the extraction and the central region.

In Fig. 37 are plotted, as a function of the radius, the first two harmonics of the field produced by the harmonic coils N. 2 and N. 19 at an excitation of 100 A.

The harmonic content of the field decreases slowly with the order of the harmonic and therefore the first and second harmonics have approximately the same order of magnitude and the same phase.

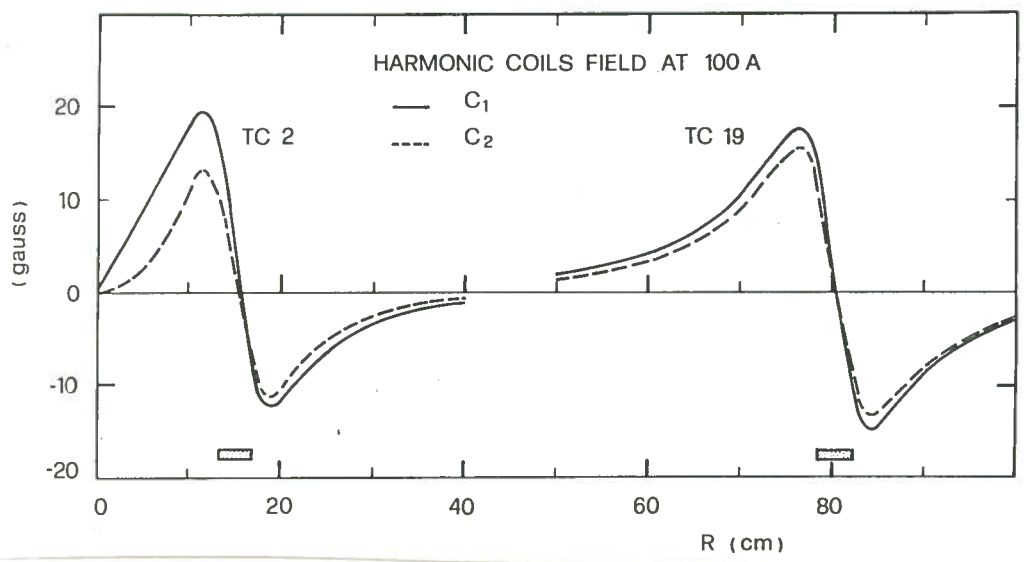

FIG. 37 - Harmonics C_1 and C_2 of two trim coils when operated in the harmonic mode at 100 A of excitation.

Some selected form factors for the first harmonic produced by the harmonic coils (1, 2), (3, 4) and (19, 20) are presented in Figs. 38, 39 and 40 as a function of the radius. The form factors are normalized to a maximum of 20 gauss and 10 gauss respectively and the required excitations in the coils, and their radial location, are also indicated. As apparent from the figures a wide selection of form factors is possible, characterized by the radius where the peak amplitude occurs (variable approximately within $\pm$ 3 cm) and by the residual perturbation at the inner and outer radii.

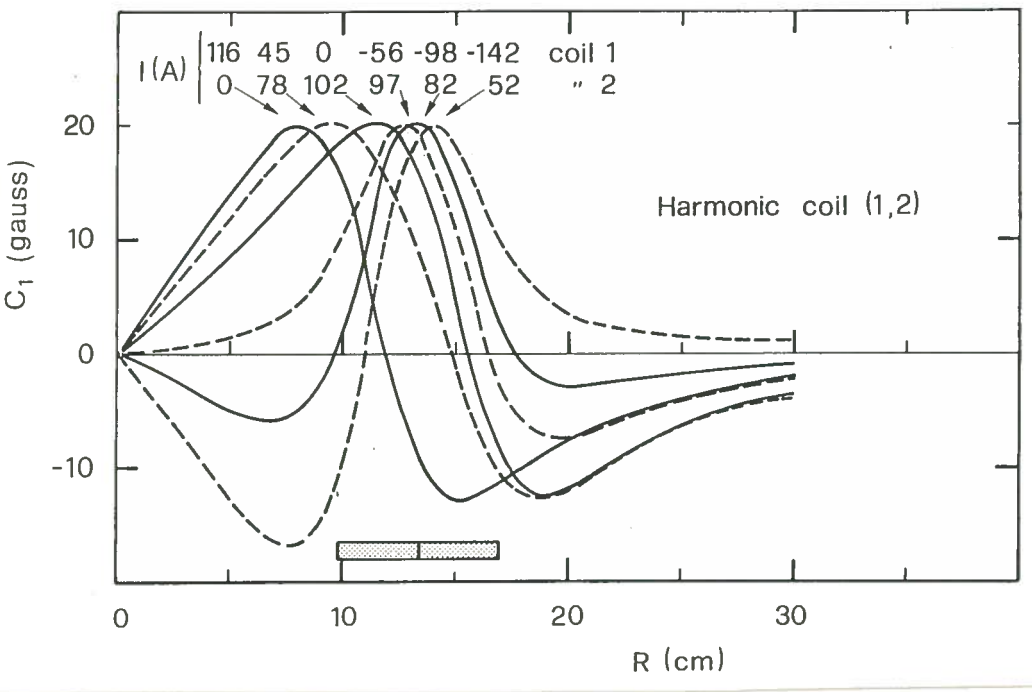

FIG. 38 - First harmonic form factors of the harmonic coil (1, 2) with the peak value normalized at 20 gauss. The required excitations are also indicated.

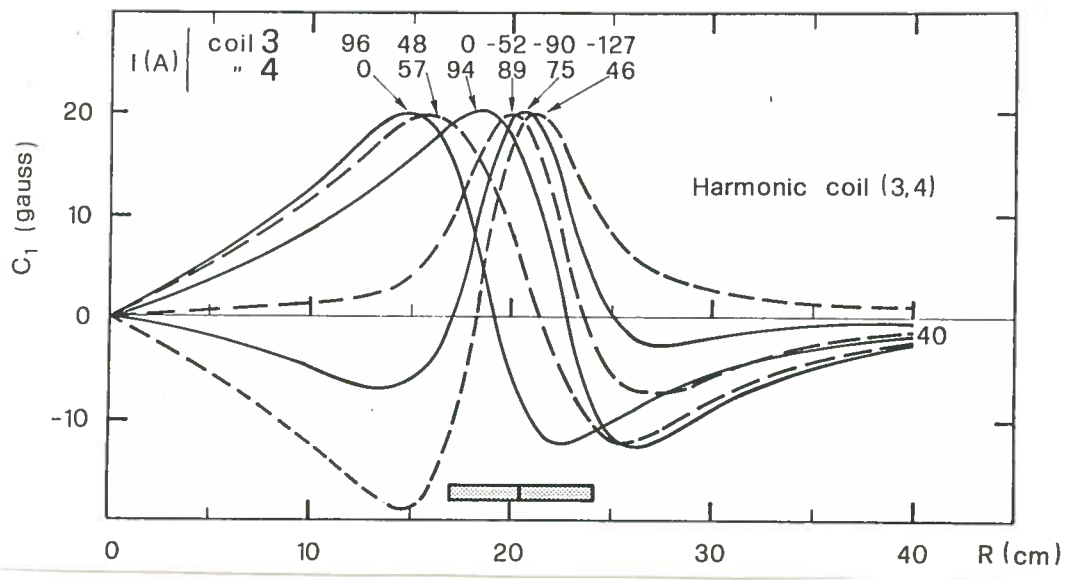

FIG. 39 - First harmonic form factors of the harmonic coil (3, 4) with the peak value normalized at 20 gauss. The required excitations are also indicated.

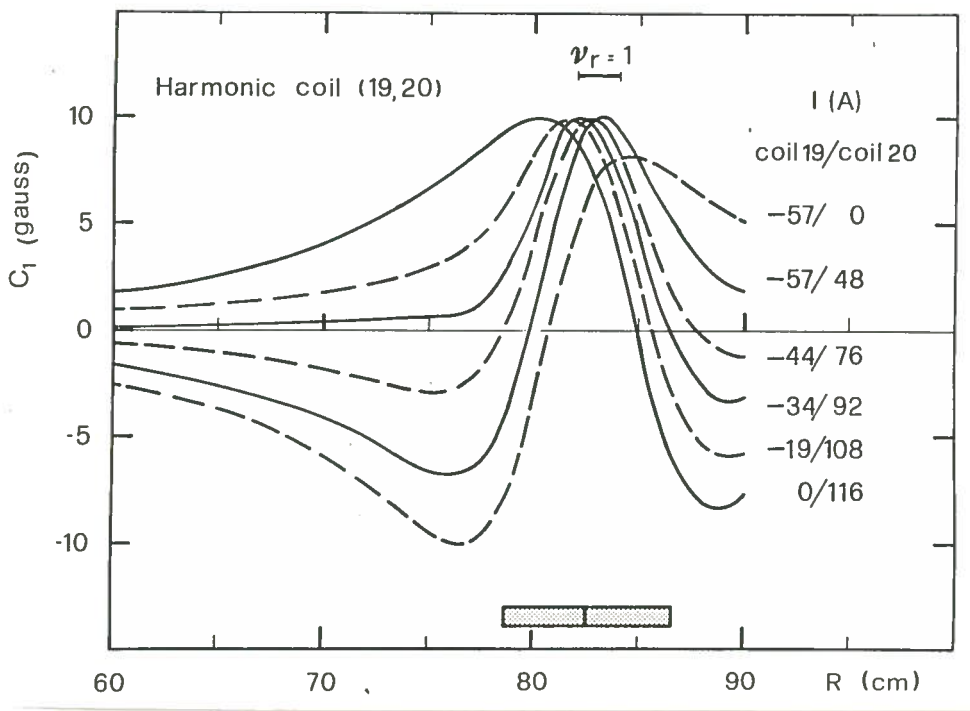

FIG. 40 - First harmonic form factors of the harmonic coil (19, 20) with the peak value normalized at 20 gauss. The required excitations are also indicated.

Note that it is not possible to control separately the first and second harmonic since the trim coils have a three-fold symmetry, so that the control of the first harmonic will therefore produce a second harmonic perturbation and viceversa.

The setting of the current in the coils in order to produce a first harmonic B_1^* with phase ϑ_1^* at a given radius r^* and zero average field is

$$i_k = (2/3)(B_1^*/C_1^*) \cos(\varphi_1^* - \vartheta_1^* + 120^oK)$$

where $k = 0, 1, 2$ indicates the coil location (hill n. 1, 2, 3) and C_1^*, φ_1^* are the amplitude and phase of the first harmonic form factor of the coil corresponding to $k = 0$.

The first harmonic $B_1 \cos(\vartheta - \vartheta_1)$ has therefore the radial shape

$$B_1(r) = (B_1^*/C_1^*)\, C_1(r)$$

$$\vartheta_1(r) = \varphi_1(r) + (\vartheta_1^* - \varphi_1^*) .$$

The induced second harmonic $B_2 \cos 2(\vartheta - \vartheta_2)$ is

$$B_2(r) = (B_1^*/C_1^*)\, C_2(r)$$

$$\vartheta_2(r) = \varphi_2(r) + (\varphi_1^* - \vartheta_1^*)/2 ,$$

where C_2, ϑ_2 are the amplitude and phase of the second harmonic form factor of the coil $k = 0$.

The maximum current required in the coils to produce a first harmonic with arbitrary phase and absolute peak value of 20 and 10 gauss respectively for harmonic coils (1, 2), (3, 4) and (19, 20) are therefore 2/3 of the values reported in Figs. 38, 39 and 40, as can be deduced from the above formulas. These currents are summarized in Table VII.

TABLE VII - Maximum excitations for harmonic mode operation.

Coil	I (A)	Note
1 2	98 68	Harmonic coil (1, 2) B_1 = 20 gauss
3 4	84 64	Harmonic coil (3, 4) B_1 = 20 gauss
19 20	44 78	Harmonic coil (19, 20) B_1 = 10 gauss

We point out that the max excitation possible in the harmonic mode operation is about a factor two higher than those reported in Table VII so that a considerable safety margin exists.

7. 2. - Yoke holes compensation

A fair number of holes, of variable size, are drilled across the yoke on the mid plane (see Fig. 41) in order to:

- accomodate the beam entry and exit channels;
- accomodate the radial coil supports;

- accomodate the actuators of the deflectors and of the magnetic channels, the high voltage feedthroughs and the beam probes.

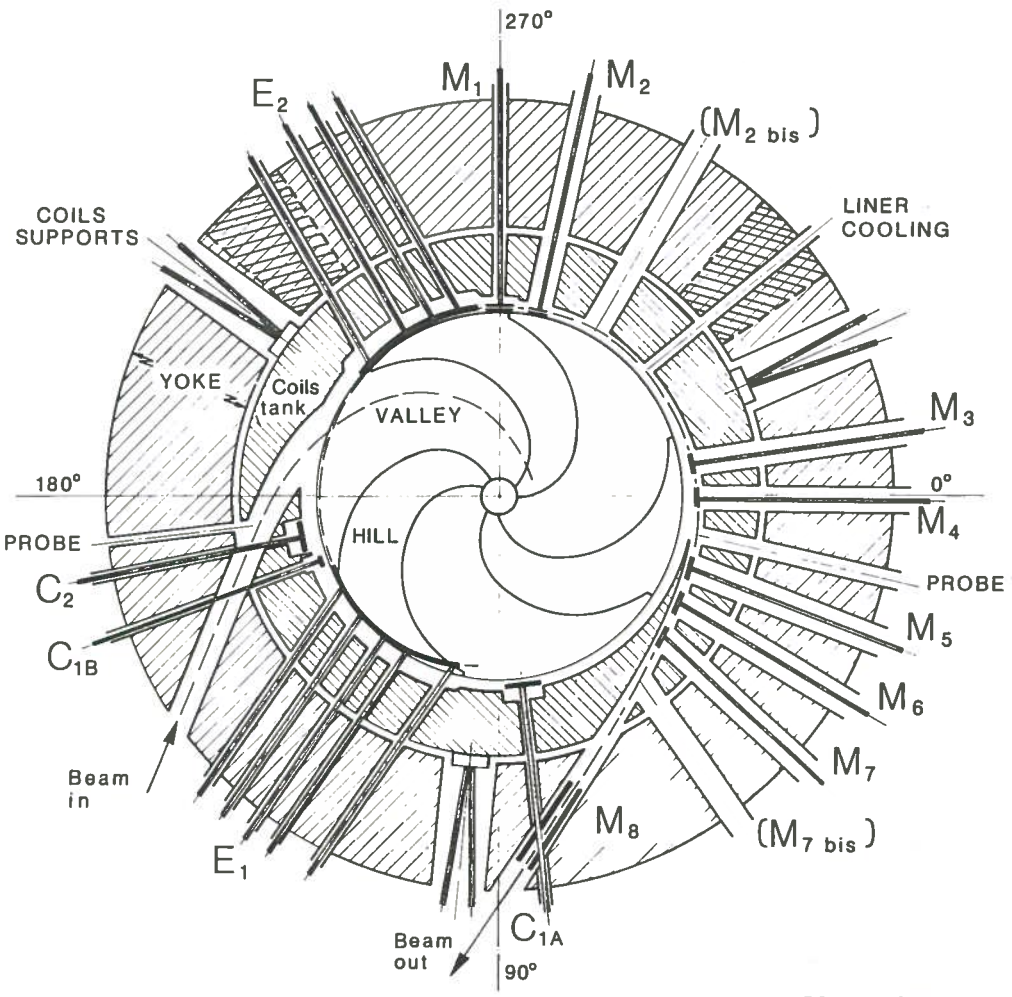

FIG. 41 - Sketch of the cyclotron median plane showing all the radial penetrations in the yoke.

The dimensions (width W and total height H) and the azimuthal positions of the yoke holes are listed in Table VIII.

The two azimuthal positions ϑ_1 and ϑ_2 of the Table when not equal indicate that the corresponding hole is not drilled radially (see for example the beam entry and exit holes) and they give therefore the position at R = 134 cm (yoke inner radius) and R = = 190 cm (yoke outer radius). The labels of the holes refer to Fig. 41.

All these holes, with the exception of the coils support holes, lack the three--fold symmetry of the pole sectors and produce therefore a first and second harmonic field perturbation. This can be dangerous at extraction, since the beam separation at the deflector entrance is obtained with the excitation of the $\nu_r = 1$ resonance.

The field perturbations produced by the yoke holes are negligible at the lowest main coils excitations but increase as the iron yoke becomes more saturated.

TABLE VIII - Yoke holes parameters.

Holes	ϑ_1 (deg) (R = 130 cm)	ϑ_2 (deg) (R = 190 cm)	W (cm)	H (cm)
M4	1	1	13	7
Probe	12	12	10	7
M5	21	21	17	7
M6	31	31	17	7
M7	41	41	17	7
M7 bis	53	53	17	7
C1A	83	83	5.8	5.8
E1	111.93	116.10	5.8	5.8
E1 H.V.	122.18	123.07	8.3	8.3
E1 H.V.	127.82	126.93	8.3	8.3
E1	134.47	131.46	5.8	5.8
E1	140.98	135.84	5.8	5.8
C1B	160	160	5.8	5.8
C2	168	168	5.8	5.8
Probe	173	173	4.3	4.3
E2	230.17	233.29	5.8	5.8
E2	240	240	5.8	5.8
E2 H.V.	246.54	244.46	8.3	8.3
E2	252.26	248.34	5.8	5.8
M1	270	270	5.8	5.8
M2	282	282	13	7
M2 bis	300	300	17	7
Liner	320	320	5.8	5.8
M3	351	351	13	7
Inj.	163.50	146.67	25	25
Extr.	68.60	87.71	25	25
S1	96	96	25	25
S2	216	216	25	25
S3	336	336	25	25

- M1, M2, M2bis, M3, M4, M5, M6, M7 and M7bis — holes provided for the actuators of the magnetic channels;
- E1 and E2 — holes for the actuators of the two deflectors;
- E1 H.V. and E2 H.V. — high voltage feedthroughs of the two deflectors;
- C1A, C1B and C2 — holes for the actuators of the compensating bars;
- Inj. and Extr. — injection and extraction holes;
- Probe and Liner — holes for beam diagnostic and liner cooling;
- S1, S2 and S3 — holes for the radial coil supports.

As shown later the first harmonic reaches very high values and therefore a compensation is necessary. The compensation is achieved by drilling in the yoke additional holes of proper volume and azimuthal location in order to minimize, or cancel out, the first and the second harmonic near the radius R = 83 cm where the beam crosses the resonance $\nu_r = 1$.

The perturbating field produced at extraction by these yoke holes is calculated assuming a uniform saturation, in the z direction, of the iron yoke. The assumption of saturation is correct since at the higher excitation of the main coil sections, i. e. 3500 A/cm^2, the field inside the yoke is well above 22 Kgauss. The uniform saturation in the z direction is not fulfilled in reality because the holes in the yoke have generally a square vertical section so that the edges (corners) effects are quite important.

No other procedure is however available since the tridimensional codes, which could in principle solve exactly the problem, cannot describe such a complicated iron configuration.

The field perturbation at R = 82 cm produced by the holes listed in Table VIII is

$$C_1 = 91.6 \text{ gauss}, \qquad \varphi_1 = 93.26^{\circ},$$

$$C_2 = 8.6 \text{ gauss}, \qquad \varphi_2 = 88.86^{\circ}.$$

The full compensation of such a perturbation requires at least two holes of proper volume and position since it involves four parameters, namely the amplitude and phase of the first and second harmonic.

The compensation can easily be achieved also with three holes. The procedure is to cancel the first (or second) harmonic with one hole and thereafter cancel the second (or first) harmonic with two equal holes 180° (or 90°) degrees apart. One can show that the three holes scheme is less efficient than the two holes scheme since it requires generally the removal of more iron from the yoke.

The first scheme has therefore been selected with the constraint of a maximum hole height of 25 cm corresponding to the height of the yoke central ring.

The position and volume of the two compensating holes were determined by an iterative Newton search. The compensating holes are indicated in Fig. 41 as cross hatched area. They are located at $\vartheta = 228.4^{\circ}$ and $\vartheta = 318.97^{\circ}$ with an azimuthal constant width of 14.1° and 13.9° respectively and an height of 25 cm as already indicated.

The compensation reduces the first and second harmonic to ~2 gauss in the region between R = 70 cm and R = 90 cm. The iron removed from the yoke has a total volume of 0.397 m^3 subdivided as follows:

coil support holes	0.106 m^3,
actuators holes	0.088 m^3,
inj. and extr. holes	0.088 m^3,
compensating holes	0.115 m^3.

The indicated volume corresponds to a removal of 25% of the iron in the yoke central ring which has a 25 cm height.

All the yoke holes will be drilled before the magnetic field measurements so that a high degree of confidence is needed for the volume and position of the compensating holes.

A rough cross check of this procedure has been carried out for a bidimensional case corresponding to roll out the yoke and assume an infinite radial yoke thickness. Four holes of different cross section, namely $W \times H = 24 \times 24\ cm^2$, $8 \times 8\ cm^2$, $16 \times 8\ cm^2$, $8 \times 8\ cm^2$, have been considered over an equivalent yoke width of 45^o. Fluxes comparable to the values calculated for the yoke (corresponding to $B = 2.05\ T$) have been applied and the two dimensional problem has been solved with the code POISSON and the uniform saturation assumption.

Scaling factors F_s for the uniform saturation approach, determined by comparing the calculated field values at the hole center, were:

hole	$W \times H = 24 \times 24\ cm^2$	$F_s = 0.56$,
	$16 \times 8\ cm^2$	$F_s = 0.87$,
	$8 \times 8\ cm^2$	$F_s = 0.84$.

These scaling factors were subsequently applied to the uniform saturation calculation of the real structure. The first and second harmonic field perturbation at extraction are of the order of 8 and 2 gauss respectively. These values, within the limit of the model adopted, assure that a good degree of compensation should be reached with the compensating holes.

8. - CONCLUSIONS

On the basis of the studies presented here the following conclusions can be drawn:

- The design values of a focusing limit $K_{FOC} = 200$ is met with good margin since minimum axial focusing frequency is $\nu_z = 0.18$. Coil operation will tell whether some margin exists also on the bending limit, as expected by critical currents data.
- The field isochronization looks excellent and the trim coils power is limited to reasonable values with generally good margins on the T. C. currents.
- The onset of the resonance $\nu_r + 2\nu_z = 3$, which limits the machine performances at the low field levels, is to some extent controlled with the radial cut of the sectors profile thus assuring a wide operating range for the magnetic field (22-48 Kgauss).
- The control of the first harmonic, either in term of reducing the field imperfection

or to excite the $\nu_r = 1$ resonance for beam extraction or centering, is provided with a wide selection of first harmonic form factors.

All these characteristics are obviously dependent on the accuracy of the calculated fields. Previous experience on the design of the MSU K500 cyclotron would indicate that with a careful design only minor modifications of the iron structure are needed after the magnetic field measurements. These modifications are required because of small differences, between calculations and measurements, in the iron field modulation as well in the radial shape of the average iron field.

Consequently the following decisions were taken:

- All the radial penetrations in the yoke and in the cryostat, for the injection and the extraction of the beam, will be machined before the magnetic field measurements.
- The trim coils will be wound on the hills leaving space, for shimming, in the central and in the extraction region. Trim coils will be in place at the time of the magnetic field measurements so that the basic field data as well as the trim coils form factors will be available.
- The passive magnetic channels will be inserted and their influence measured in the first set of field measurements.

The rationale for this choices is to reduce by a considerable amount (of the order of one year) the time required to complete the machine. One single set of magnetic field measurements will hopefully be sufficient to evaluate the possible iron modifications to produce the final magnetic field.

In view of the detail of the present study no further modifications of the overall geometry of the machine are anticipated until magnetic field measurements are carried out.

A selection of typical beams which will be accelerated by the machine is presented in Table IX. The maximum charge state, as obtained by stripping after injection from a Tandem or from an external ion source, is shown for each element together with some intermediate charge state values.

The highest energy per nucleon and the corresponding RF frequency, harmonic number, peak voltage on the dee and center field value are also listed. The expected intensities vary from 5×10^{11} for the light ions down to 2×10^{10} for the heavy ions (see ref. (2)).

TABLE IX - Typical beams.

Element	A	Z_s	T/A (MeV/n)	RF (MHz)	h	V_{dee} (kV)	B_o (Kgauss)
He	4	2	100	24.0	1	100	31.3
		1	49	17.5	1	100	45.5
C	12	6	100	24.0	1	100	31.3
		4	67	19.8	1	100	39.0
		3	49	17.5	1	100	45.5
O	16	8	100	24.0	1	100	31.3
		6	75	21.1	1	100	36.6
		4	49	17.5	1	100	45.5
Ne	20	10	100	24.0	1	100	31.3
		7	70	20.4	1	100	38.0
		5	49	17.5	1	100	45.5
S	32	16	100	24.0	1	100	31.3
		12	75	21.1	1	100	36.6
		8	49	17.5	1	100	45.5
Ar	40	18	90	22.8	1	100	33.0
		14	70	20.4	1	100	38.0
		9	41	15.9	1	97	46.0
Ca	40	18	90	22.8	1	100	33.0
		15	75	21.1	1	100	36.6
		10	49	17.5	1	100	45.5
Kr	84	23	55	18.3	1	100	43.5
		17	33	28.8	2	89	46.3
		11	14	19.0	2	60	47.3
J	127	28	39	15.8	1	95	46.0
		22	24	24.8	2	77	46.7
		14	10	16.1	2	51	47.5
Xe	132	29	39	15.5	1	95	46.0
		22	22	24.0	2	75	46.8
		15	11	16.6	2	52	47.5
Ta	181	34	28	26.8	2	83	46.5
		25	16	20.0	2	63	47.2
		17	7	20.6	3	65	47.6
Au	197	35	26	25.5	2	79	46.7
		26	14	19.2	2	60	47.3
		17	6	18.9	3	60	47.6
Pb	208	36	24	24.9	2	77	46.8
		26	13	18.2	2	57	47.4
		17	5	18.0	3	57	47.7
U	238	38	21	23.0	2	72	47.0
		28	11	17.1	2	54	47.4
		19	5	17.5	3	56	47.7

- A and Z_s Mass number, charge state;
- T/A Maximum energy per nucleon;
- RF and h RF frequency, harmonic number;
- V_{dee} Peak voltage on the dee;
- B_o Center field level for the maximum energy per nucleon.

REFERENCES

(1) - E. Acerbi et al., Studio del progetto di un ciclotrone superconduttore per ioni pesanti, Report INFN (1976).

(2) - E. Acerbi et al., The Milan Superconducting Cyclotron Project, Proceedings of the IX Intern. Conf. on Cyclotron and their Applications, Caen (France) 1981 (Les Editions de Physique, 1981), p. 169.
- E. Acerbi et al., Status of the Superconducting Cyclotron Project in Milan, XIX European Cyclotron Progress Meeting, Grenoble (France) 1982; Report INFN/ /TC-82/12 (1982).
- E. Acerbi et al., Status of the Milan Superconducting Project, Proceedings of the 1983 Particle Accelerator Conference, IEEE Trans. on Nuclear Sci. NS-30, 2126 (1983).

(3) - C. De Martinis and D. Giove, The magnet structure of the Milan Superconducting Cyclotron, Report INFN/TC (to be published).

(4) - E. Acerbi et al., Design of the Main Coils for the Milan Superconducting Cyclotron, Proceedings of the IX Intern. Conf. on Cyclotron and their Applications, Caen (France) 1981 (Les Editions de Physique, 1981), p. 399.
- E. Fabrici, Magnetic Forces on the Coils of the Superconducting Cyclotron at the University of Milan, Report INFN/TC-82/10 (1982).
- E. Acerbi et al., Current Leads System for a Superconducting Cyclotron, Proceedings of the VIII Intern. Conf. on Magnet Technology, 1983 (to be published).
- E. Acerbi and L. Rossi, Pressure Calculations for the Cryostat of the Milan Superconducting Cyclotron, Report INFN/TC-83/21 (1983).

(5) - G. Bellomo and L. Serafini, A Study of the Magnetic Forces acting on the Trim Coils for the Milan Superconducting Cyclotron, Report INFN/TC-83/7 (1983).

(6) - E. Acerbi et al., Model Studies for the Superconducting Cyclotron Project in Milan, IEEE Trans. on Nuclear Sci. NS-26, 2048 (1979).
- E. Acerbi et al., Field Measurements on the Milan Superconducting Model Magnet, IEEE Trans. on Nuclear Sci. NS-26, 2114 (1979).
- C. Pagani and G. Varisco, Model Studies of the RF Cavity for the Milan Superconducting Cyclotron, IEEE Trans. on Nuclear Sci. NS-26, 2182 (1979).

(7) - G. Bellomo, Design of the Injection System for the Milan Superconducting Project, Report INFN/TC (to be published).

(8) - E. Fabrici and A. Salomone, The Extraction System for the Superconducting Cyclotron at the University of Milan, Proceedings of the IX Intern. Conf. on Cyclotron and their Applications, Caen (France) 1981 (Les Editions de Physique, 1981), p. 501.
- E. Fabrici and A. Salomone, The Extraction System for the Milan Superconducting Cyclotron, Report INFN/TC (to be published).

(9) - G. Bellomo and F. Resmini, A Method for Minimizing the Trim Coils Power Requirements in Superconducting Cyclotrons, IEEE Trans. on Nuclear Sci. NS-26, 2095 (1979).

(10) - G. Bellomo et al., Magnetic Field Mapping of the K-500 Cyclotron at MSU, Nuclear Instr. and Meth. 180, 285 (1981).

(11) - M. M. Gordon and D. A. Johnson, Calculation of Fields in a Superconducting Cyclotron assuming Uniform Magnetization of the Pole Tips, Particle Accelerators 10, 217 (1980).

(12) - R. F. Holsinger and C. Iselin, POISCR the CERN-Poisson Program Package, CERN Report (unpublished).
- E. Fabrici and F. G. Resmini, Poisson Calculations for the Milan Superconducting Cyclotron, Report INFN/TC (to be published).

(13) - M. M. Gordon, Calculations of Isochronous Fields for Sector Focused Cyclotrons, Particle Accelerators 13, 67 (1983).

(14) - A. Salomone, The Central Region of the Milan Superconducting Cyclotron using an Internal Ion Source, Report INFN/TC-83/13 (1983).

(15) - E. Fabrici and A. Salomone, Acceleration Studies for the Milan Superconducting Cyclotron, Report INFN/TC-83/9 (1983).

(16) - E. Acerbi, Private comunication.